NUMERICAL STUDY OF HIGHWAY NOISE BARRIER EFFECTS ON POLLUTANT DISPERSION

by

Liyuan Gong

A Thesis

Submitted to the Faculty of Purdue University

In Partial Fulfillment of the Requirements for the degree of

Master of Science in Mechanical Engineering

Department of Mechanical and Civil Engineering

Hammond, Indiana

December 2018

THE PURDUE UNIVERSITY GRADUATE SCHOOL
STATEMENT OF COMMITTEE APPROVAL

Dr. Xiuling Wang, Chair

Department of Mechanical & Civil Engineering

Dr. Harvey Abramowitz

Department of Mechanical & Civil Engineering

Dr. Chandramouli Viswanathan Chandramouli

Department of Mechanical & Civil Engineering

Approved by:

Chenn Q Zhou

Head of the Graduate Program

ACKNOWLEDGMENTS

My sincere gratitude goes first to my advisor, Dr. Xiuling Wang, for her constant encouragement and guidance. She provided me much precious knowledge and valuable advice for this thesis. Her patience and passionate attitude towards academic work is the goal I will pursuit for the rest of my research and career.

Secondly, I would like to give my thanks to all the Professors in the department of Mechanical Engineering in Purdue Northwest. The courses I took in the past years helps a lot for this research. Especially for Dr. Harvey Abramowitz and Dr. Chandramouli Viswanathan Chandramouli who are willing to be the members of examining committee.

Finally, my thanks would go to my beloved family and friends, for their understanding, support and love.

TABLE OF CONTENTS

LIST OF TABLES

LIST OF FIGURES

NOMENCLATURE

t	time
k	turbulent kinetic energy
ε	turbulence dissipation rate
ω	specific dissipation
ρ	density
u	velocity
μ	viscosity
G_k	generation of turbulence kinetic energy due to the mean velocity gradients
G_b	generation of turbulence kinetic energy due to buoyancy
Y_M	contribution of the fluctuating dilatation in compressible turbulence to the overall dissipation rate
σ_k	turbulence Prandtl number for k
σ_ε	turbulence Prandtl number for ε
S_k	user-define source term
S_ε	user-define source term
S_ω	user-define source term
G_ω	generation of ω
Γ_k	effective diffusivity of k
Γ_ω	effective diffusivity of ω
Y_k	dissipation of k due to turbulence
Y_ω	dissipation of ω due to turbulence
D_ω	cross-diffusion term
$\bar{S}_{ij}$	rate-of-strain tensor for the resolved scale
v_t	subgrid-scale turbulent viscosity
p	pressure
ψ_h	non-dimensional function

Y_i local mass fraction of species i

R_i net rate of production of species i by chemical reaction

S_i rate of production from sources

p power law exponential rate

h height

κ Von Kármán constant

z_{ref} reference height

U_{ref} velocity at referebce height

L Monin-Obukhov Length

ψ stability term in Logarithmic law

θ_* absolute ambient temperature

θ_0 ground level temperature

$\theta(z)$ temperature at different heights

ABSTRACT

Author: Gong, Liyuan. MSME
Institution: Purdue University
Degree Received: December 2018
Title: Numerical Study of Highway Noise Barrier Effects on Pollutant Dispersion
Major Professor: Xiuling Wang

Roadside noise barrier helps to reduce downwind pollutants concentration from vehicle emission. This positive characteristic of the construction feature can be explained by its interaction with flow distribution and species transportation. In this thesis, 3-D numerical model has been developed to simulate highway pollutant transportation - realizable k-e model was employed to model turbulent flow; non-reaction species dispersion was applied to simulate species transport. First, numerical models were validated with experimental data. Good agreement was observed. Then detailed simulations were conducted to study double barriers' effects on highway pollutant dispersion under different settings: noise barriers with different heights, noise barriers with and without edge effects, different atmospheric thermal boundary conditions. Results show that: (1) Noise barrier feature helps reduce downwind pollutant concentration. For 4m tall double barriers without edge effect case, 80% less concentration can be found than non-barrier case at downwind 100m; (2) Reduction of concentration increases as barrier height increases. 1m higher can lead 0.002 $^{mol}/_{m^3}$ more concentration reduction at ground level. (3) Unstable condition has the least concentration and stable condition has the highest concentration at the same location. (4) Barrier with edge effect has higher concentration than barrier without edge effect downwind; (5) Oblique wind condition enlarges barrier edge effect. The larger the oblique angle is, the higher turbulence intensity can be found near barrier edges. These findings will be provide valuable input to noise barriers design so as to improve roadside neighborhood air quality.

1. INTRODUCTION

1.1 Motivation

Vehicle exhausts contributes highly to air pollution and causes the increase of fatal diseases, lower birth rate and other health problems. Air quality near roadway is highly related to passing vehicles emission rate. This has been a deteriorating problem that is threatening human and animal's health in the vicinity of a busy roadway. China has been suffering from severe air pollution for the past decades. 70% is contributed by motorized vehicle emission [1]. As a matter of fact, air pollution has been a consistent and vital issue spreading all around the world. According to EPA, motor vehicles overall cause nearly 75% of carbon monoxide pollution in the U.S. [2]. Moreover, over 45 million people in the U.S. are estimated to live, work or attend school within 300 feet of roadways where high concentrations of air pollution have been observed due to motor vehicle. It is crucial to study highway contaminant dispersion and methods to minimize the exposure to air pollution caused by vehicle emission.

Noise barrier feature has been originally constructed to prevent moving vehicle noise from neighborhood located near roadside. Studies have suggested roadside barriers have positive effects on reduction of downwind pollutant concentration. The level of benefits can be influenced by many factors. Such as roadway configuration, local meteorology, barrier height design, endpoint location edge effects and other factors [3]. Further detailed and multiple forms of studies are necessary for understanding all effects of determination factors. It will provide more suitable suggestions on the range of options for roadside barriers design. It will assist future roadside construction and new technology creation for improving air quality.

1.2 Literature Review

Studies related to noise barrier effects on air pollution dispersion have been done in various formats. Some of the well-known methods are wind tunnel experiments, field data collection and analysis and simulations to understand relations between factors, and to create or modify analytical computation models or numerical models.

A frequently referred wind tunnel experiment was described in Heist et al 2009. It focused on the analysis of roadway elevation or depression effects combined with different barriers heights. It emphasized on the importance of considering roadway configuration into studying of near road quality and demonstrated that combining virtual origin shift and entrainment velocity function, as well as roadway geometry is effective for modeling different types of roadway configurations [4].

Field study is another popular approach to study similar topics. It gives us more accurate realistic and practical real time data for further modeling and analysis. In Baldauf et al 2009, study focused on the effects of noise barriers design on contaminant concentration downwind by analyzing data collected. It also gives an insight of relation between roadside design with contaminant plume rise based on Heist wind tunnel data [5]. Similar results were suggested in Ning et al 2010. A contaminant concentration peak was found downwind about 1.9-2.2 times of that at clearing site [6]. Another field study done by Hagler 2012, it studied barriers effect under various wind conditions [7]. Then in Finn et al 2009, a study on noise barrier effect under various atmospheric stability conditions was done by a tracer experiment [8]. In Baldauf et al 2016, a field experiment was done to study barrier height effect combining with roadside vegetation. Results have shown that roadside vegetation can be the secondary barrier to pollutant dispersion. It suggests more trees can assist in barriers effects on reducing air pollution downwind [9].

Numerical simulation comparing with field study and wind tunnel experiments is relatively more time saving and cost efficient. Many researchers have used CFD or other numerical methods to study similar topics related to noise barrier effects on air pollution. In Hagler 2011, CFD method was used to study barriers height effects and different wind directions [10]. Schulte et al 2014

evaluated the ability of two numerical models for studying barriers height effects under different thermal stabilities [11]. In most recent studies, Lee 2017 et. al,. studied the combination of noise barrier and roadside vegetation effects on air pollution dispersion under various wind conditions based on a field study [12]. Heist 2018, studied effect of depressed roadway configurations modeling vehicle emission gases dispersion [13]. Noise barrier edge effect was first mentioned in Steffen 2013. Sensitivity study of wind angle and wind speed on effect of barriers edge effect was studied. It described that edge effect might cause secondary recirculation and came up with conclusion that edge effect gets stronger with higher wind speed [14]. However, there were no further detailed analyses or results on noise barrier edge effects on pollutant dispersion and how edge effect is influenced by wind speed and thermal effects.

This study continuously used a CFD simulation method to study barrier edge effects. It focused on barrier edge effects at different inlet wind speed, barrier heights and various atmospheric thermal stability conditions. The purpose of this study is to visualize barriers height and edge effects on flow and pollutants dispersion near roadside; to study overall influence of atmospheric thermal effects and barriers configurations; to serve as a continuous study on barrier edge effects concept; to propose and suggest future study trends and potentials. RANS method was used to simulate height effects and edge effects study first.

2. NUMERICAL MODELING AND VALIDATION

2.1 Turbulence Modeling

Turbulence models seek to solve a modified set of transport equations by introducing averaged and fluctuating components. The basic of turbulence numerical modeling is to solve Navier-Stokes equations. The continuity equation, momentum equation and energy equation is introduced as below:

The three-dimensional-unsteady Navier-Stokes Equations are:

Continuity: $$\frac{\partial \rho}{\partial t} + \frac{\partial (\rho u)}{\partial x} + \frac{\partial (\rho v)}{\partial y} + \frac{\partial (\rho w)}{\partial z} = 0 \quad (1)$$

X-Momentum: $$\frac{\partial (\rho u)}{\partial t} + \frac{\partial (\rho u^2)}{\partial x} + \frac{\partial (\rho uv)}{\partial y} + \frac{\partial (\rho uw)}{\partial z} = -\frac{\partial p}{\partial x} + \frac{1}{Re_r}\left[\frac{\partial \tau_{xx}}{\partial x} + \frac{\partial \tau_{xy}}{\partial y} + \frac{\partial \tau_{xz}}{\partial z}\right] \quad (2)$$

Y-Momentum: $$\frac{\partial (\rho v)}{\partial t} + \frac{\partial (\rho uv)}{\partial x} + \frac{\partial (\rho v^2)}{\partial y} + \frac{\partial (\rho vw)}{\partial z} = -\frac{\partial p}{\partial y} + \frac{1}{Re_r}\left[\frac{\partial \tau_{xy}}{\partial x} + \frac{\partial \tau_{yy}}{\partial y} + \frac{\partial \tau_{yz}}{\partial z}\right] \quad (3)$$

Z-Momentum: $$\frac{\partial (\rho w)}{\partial t} + \frac{\partial (\rho uw)}{\partial x} + \frac{\partial (\rho vw)}{\partial y} + \frac{\partial (\rho w^2)}{\partial z} = -\frac{\partial p}{\partial z} + \frac{1}{Re_r}\left[\frac{\partial \tau_{xz}}{\partial x} + \frac{\partial \tau_{yz}}{\partial y} + \frac{\partial \tau_{zz}}{\partial z}\right] \quad (4)$$

Energy: $$\frac{\partial (E_T)}{\partial t} + \frac{\partial (uE_T)}{\partial x} + \frac{\partial (vE_T)}{\partial y} + \frac{\partial (wE_T)}{\partial z} = -\frac{\partial (up)}{\partial x} - \frac{\partial (vp)}{\partial y} - \frac{\partial (wp)}{\partial z} - \frac{1}{Re_r Pr_r}\left[\frac{\partial q_x}{\partial x} + \frac{\partial q_y}{\partial y} + \frac{\partial q_z}{\partial z}\right] + \frac{1}{Re_r}\left[\frac{\partial}{\partial x}\left(u\tau_{xx} + v\tau_{xy} + w\tau_{xz}\right) + \frac{\partial}{\partial y}\left(u\tau_{xy} + v\tau_{yy} + w\tau_{yz}\right) + \frac{\partial}{\partial z}\left(u\tau_{xz} + v\tau_{yz} + w\tau_{zz}\right)\right] \quad (5)$$

The N-S equations can be solved directly by the finite difference method and spectral method. This method is called Direct Numerical Simulation (DNS) and it can solve all the turbulent problems. However, it is only applicable to low Reynolds number cases due to its high requirements on computational cost.

Two common mathematic models are applied to solve the N-S equations: the Reynolds Average Navier-Stokes (RANS) model and Large Eddy Simulation (LES) model. The RANS model computes for a time averaged quantities. It is more suitable for smaller Reynolds number and low turbulence level. LES models solves for large eddies. It filters out scales that are smaller than meshing scale. It requires larger computational effort and time.

Realizable k-ε model is used as turbulence flow model in this study. This model is developed based on standard k-ε model. It solves turbulence flow field by introducing two parameters: Turbulence Kinetic Energy (TKE) & Turbulence Dissipation Rate (TDR). These two terms are added to standard k-ε model equation to complete a close formula. The transport equations for realizable k-ε model are:

$$\frac{\partial}{\partial t}(\rho k) + \frac{\partial}{\partial x_j}(\rho k u_j) = \frac{\partial}{\partial x_j}\left[\left(\mu + \frac{\mu_t}{\sigma_k}\right)\frac{\partial k}{\partial x_j}\right] + G_k + G_b - \rho\varepsilon - Y_M + S_k \quad (6)$$

And

$$\frac{\partial}{\partial t}(\rho \varepsilon) + \frac{\partial}{\partial x_j}(\rho \varepsilon u_j) = \frac{\partial}{\partial x_j}\left[\left(\mu + \frac{\mu_t}{\sigma_\varepsilon}\right)\frac{\partial \varepsilon}{\partial x_j}\right] + \rho C_1 S\varepsilon - \rho C_2 \frac{\varepsilon^2}{k+\sqrt{v\varepsilon}} + C_{1\varepsilon}\frac{\varepsilon}{k}C_{3\varepsilon}G_b + S_\varepsilon \quad (7)$$

Where,

$$C_1 = max\left[0.43, \frac{\eta}{\eta+5}\right], \eta = S\frac{K}{\varepsilon}, S = \sqrt{2S_{ij}S_{ij}} \quad (8)$$

Schmidt number was chosen to be 0.7 same as Masoud et al. 2017 [15]. Below Figure 1 shows comparisons by using different Schmidt number 0.4, 0.7 & 1.

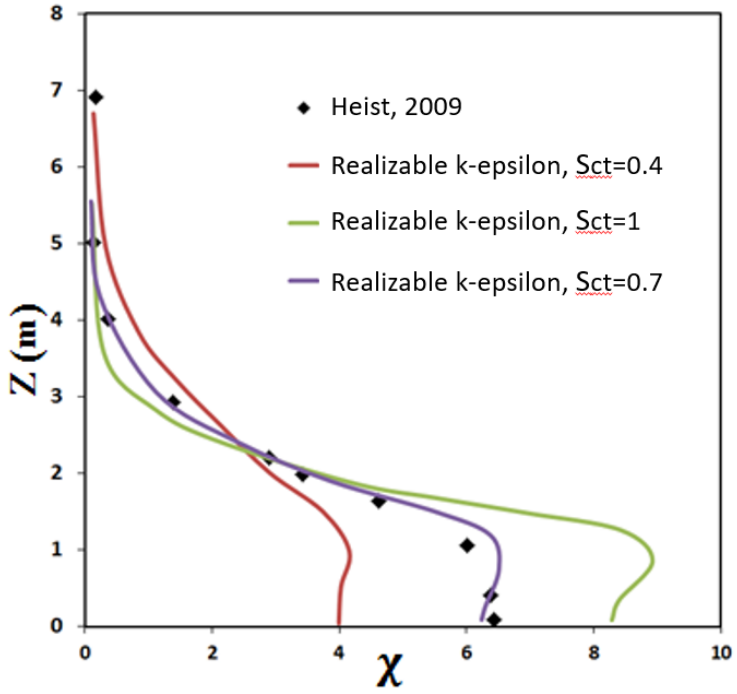

Figure 1: Comparison of vertical distribution of concentration behind solid barrier

2.2 Inlet Wind Profile

Inlet power law wind profile under neutral condition was the same as the one used by Steffens et al. in 2013.

$$U(z) = U_{ref}(z/z_{ref})^{p}, \quad (9)$$

U_{ref} is reference velocity at reference height z_{ref}. p is the exponential rate 1/7 in this study. Velocity was validated as u= 7.44 m/s (z=3m), u = 10.75 m/s (z=30m).

Computational domain for wind profile validation is shown in Figure 2. Comparison of vertical velocity distribution at 24 meters downwind is shown in Figure 3. Results were compared with Steffens's and Near Road Tracer Study (NRTS08) experimental data and simulation results by using RANS turbulence model. Velocity profile in this study has a great similarity to reference velocity profile. The line trend falls very close to the experimental data trend.

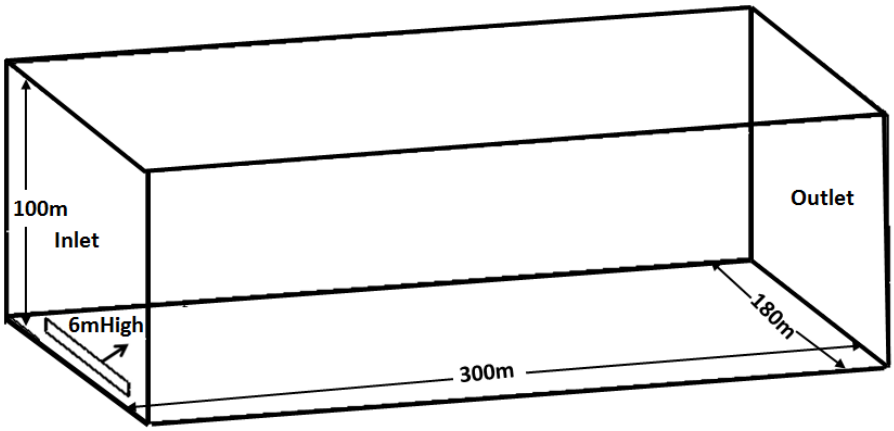

Figure 2: Computational domain for wind inlet validation

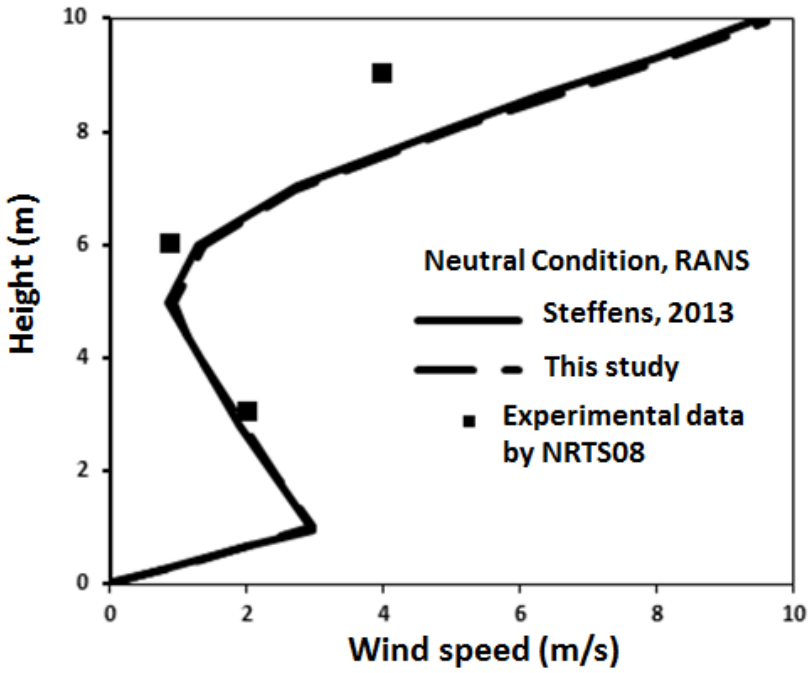

Figure 3: Wind inlet profile comparison at 24m downwind

2.3 Inlet Temperature Profiles for Different Thermal Conditions

Atmosphere boundary layer has different thermal stabilities due to the change of air temperature deviations. The change in temperature between ambient has impacts on pollutant dispersion due to buoyance effects. In this study, the inlet flow properties for large ABL domain fully developed flow are based on methods introduced in Pieterse, 2013 [16]. It assumes the flow over surface layer of a homogenous flat terrain. Basic flow properties is based on Monin-Obukhov similarity theory, describes dimensionless mean flow and mean temperature in the surface layer under non-

neutral conditions as a function of the dimensionless height parameter z/L. Where, L is defined as Monin-Obukhov length has the following form:

$$L = \frac{u_*^2 T_0}{\kappa g \theta_*}, \tag{10}$$

K is the von Karman constant, set to be 0.41 in this study. θ_* is scaling temperature discretizes neutral, stable and unstable atmosphere stability conditions.

Inlet temperature profile are given as [17]: (Alinot and Masson 2002)

$$\theta(z) - \theta_0 = (\frac{\theta_*}{\kappa})[\ln\left(\frac{z}{z_0}\right) - \psi_h(\frac{z}{L})] \tag{11}$$

where u_* is friction velocity. $\psi_h(\frac{z}{L})$ is given by:

$$\psi_h = -5\frac{z}{L}, L > 0, \tag{12}$$

$$\psi_h = 5\frac{z}{L}, L > 0, \tag{13}$$

$$\psi_h = 2\ln\left(\frac{1+x^2}{2}\right), L < 0 \tag{14}$$

$$x = (1 - 16\frac{z}{L})^{1/4} \tag{15}$$

Figure 4 shows comparisons of the inlet vertical temperature distributions against theoretical data and simulation results introduced in Pieterse et al.

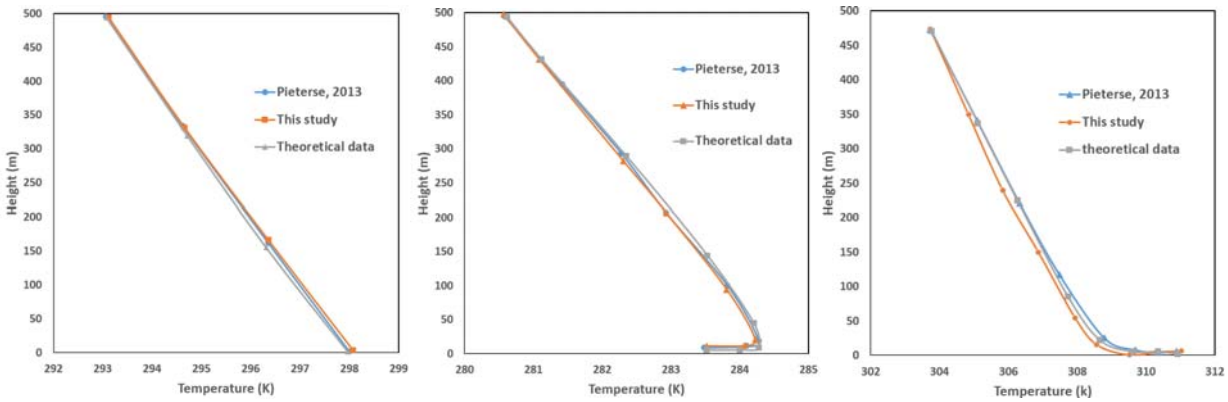

(a) Neutral Condition (b) Stable condition (c) Unstable Condition

Figure 4: Inlet temperature profile comparison results

2.4 Species Transportation Model

In order to validate contamination dispersion model used in this study, simulation settings were similar to the wind tunnel experiment introduced in Heist, 2009. SF6 emission source has a mass flow rate of 0.01kg/s. Inlet turbulent properties profiles are modified according to wind tunnel experiment input data. Numerical computation equation for non-reaction species dispersion is given by default as below:

$$\frac{\partial}{\partial t}(\rho Y_i) + +\nabla \cdot (\rho \bar{v} Y_i) = -\nabla \cdot \vec{J_i} + R_i + S_i, \quad (16)$$

Y_i is the local mass fraction of the species. R_i is the net rate of production of species i by chemical reaction, which equals to 0 in this study. S_i is the rate of production from sources. This equation follows the similar continuity equation format as Eulerian dispersion model, which specifies contaminant in molar concentration mol/m^3 instead of mass fraction [18].

Carbon Dioxide (CO_2) is the representative gasoline passenger cars and diesel trucks emission gases defined as contaminant sources in this paper. Emission mass flow rate for both gases was approximately 0.006 kg/s calculated by using the average CO_2 emission data from United States Environmental Protection Agency (US EPA) 2017 Carbon Dioxide Emissions and Fuel Economy Trends Report [19]. Average CO_2 emission rate is 0.0002kg/m (352g/mi). Vehicle highway speed estimated to be 30m/s (65mph).

Figure 5 shows the comparison of the normalized concentration versus the change of the dimensionless downwind distance x/h at ground level height z = 1m, where h represents the height of the noise barrier.

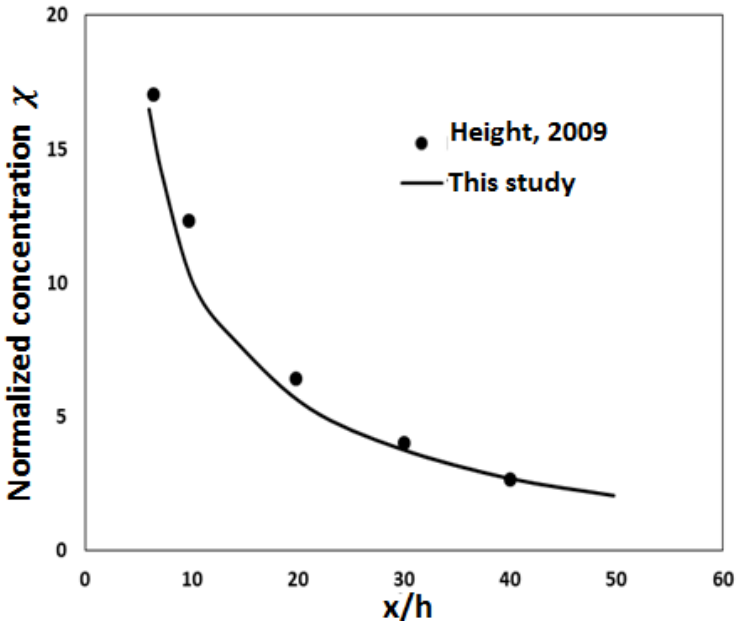

Figure 5: Normalized concentration comparisons with experimental data at ground level

A great similarity was found for all inlet conditions comparing with experimental and theoretical data. Validated simulation inlet wind profile, inlet temperature profile, and species transport model were proved can be used for further study in this research.

3. COMPARISON OF DOUBLE BARRIERS AND SINGLE BARRIERS EFFECTS ON POLLUTANT DISPERSION

3.1 Problem Description

Previous studies have shown noise barriers can help reduce downwind pollutant concentration. This contribution is affected by barriers height. People have done researches about noise barrier height effects on pollutants dispersion. In Amini et al. 2014. It was found that 4m barrier can help reduce 35% pollutant concentration. This reduction can be doubled is 55% if barrier height is doubled [20]. This study focused on barriers height effects for both double barriers and downwind single barrier configuration. The heights studied are: 1m, 2m, 3m, and 4m. Various thermal effects were also introduced to study for neutral, stable, and unstable atmospheric boundary conditions.

Figure 6 shows the geometries for single downwind and double barriers cases used in this study.

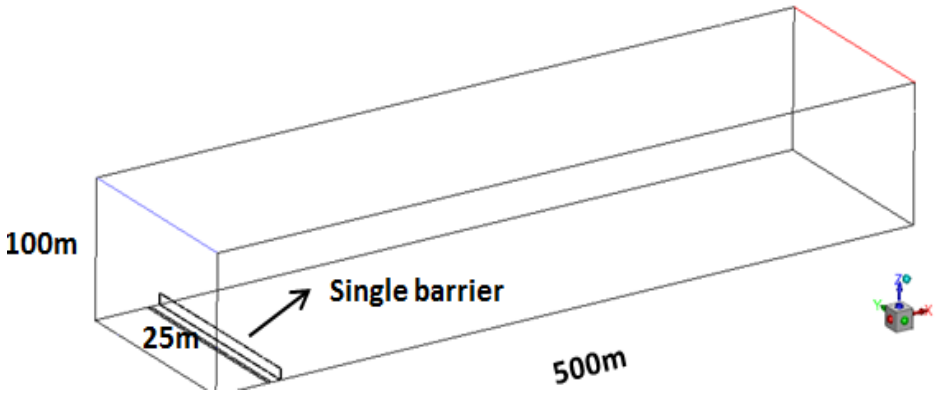

(a) Downwind single barrier computational domain

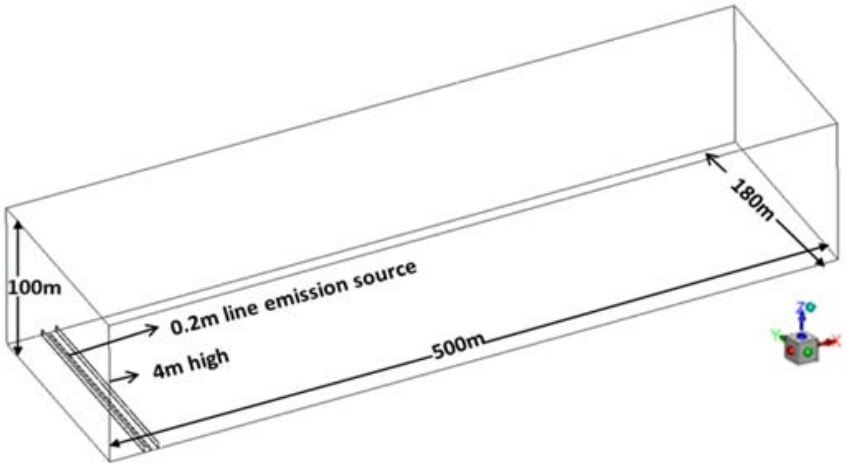

(b) Double barriers computational domain

Figure 6: Computational Domain in this Study for two Barriers configurations

Figure 7 shows mesh quality for double barriers computational domain near noise barrier and roadside emission source area. Geometry was sliced to multiple sections with 0.005 increments in mesh size. The maximum face size for section near emission source is 0.01m. The adjacent section has maximum mesh face size of 0.015m. The next adjacent section has mesh face size of 0.02m. The largest maximum face size of entire domain is 0.03m. Total meshing quantity is about 1 millions.

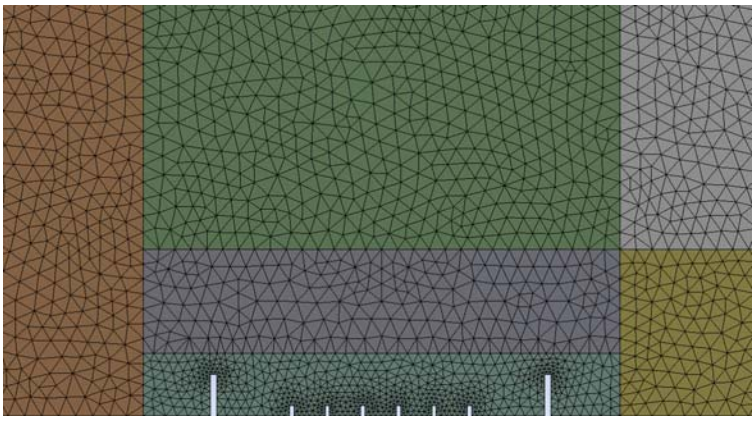

Figure 7: Mesh quality for double barrier domain

The mesh sensitivity study is applied to make sure the simulation results can be independent of meshing scale. Three different mesh quantities are applied to generate meshes with different total numbers of elements of 0.5 million, 1 million, 1.2 million. Figure 8 shows the results of velocity distribution of different meshing sizes at ground level through entire domain. Table 1 shows velocity magnitude at different downwind location at ground level for three mesh sizes. Results show that after mesh total quantity reaches above 1 million, the velocity profile maintains similar. From Table 1, velocity magnitude at different locations also stays very close. The largest velocity magnitude difference between 1 million and 1.2 million is 1.8%. In order to guarantee calculation efficient and meshing quality, total of 1 million meshing was finalized for this study.

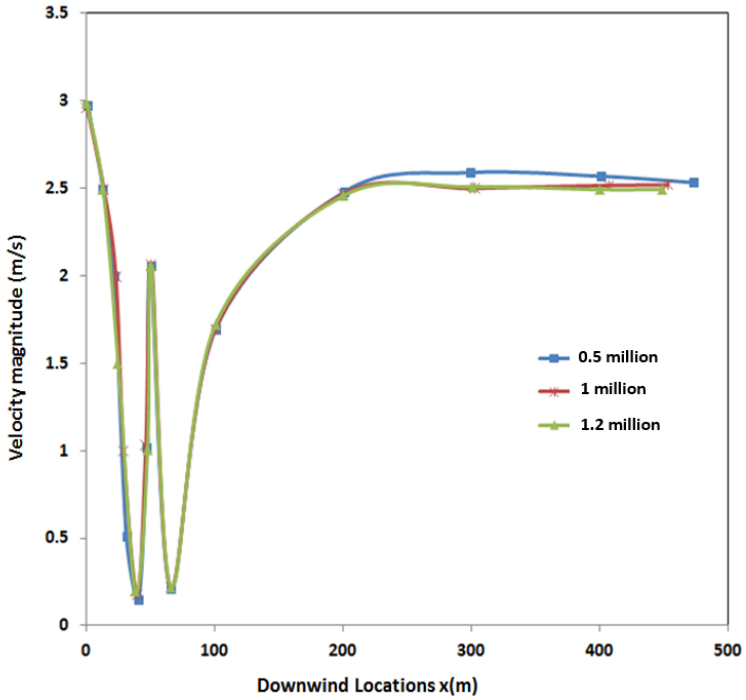

Figure 8: Mesh sensitivity study of velocity magnitude at ground level for different meshing scales

Table 1: Velocity magnitude comparison at downwind locations for two meshing scales

Downwind locations / Mesh sizes	X=50m	X=100m	X=200m	X=300m	X=500m
1 million	0.189	1.695	2.458	2.508	2.500
1.2 million	0.191	1.713	2.462	2.511	2.500
Difference (%)	0.2	1.8	0.4	0.3	0

3.2 Noise Barrier Height Effects on Pollutant Dispersion

In this section, simulation results of flow characteristics such as velocity magnitude, turbulence intensity and turbulence kinetic energy (TKE) are compared between single downwind barrier and double barriers geometries with various barriers height under neutral condition in order to show the height effects on flow field properties.

Figure 9 shows flow velocity contour at mid plane for downwind single barrier and double barrier cases below 10m under neutral condition. The maximum velocity magnitude can reach up to 5m/s. Plotted horizontal span ranges from inlet to downwind 100m.

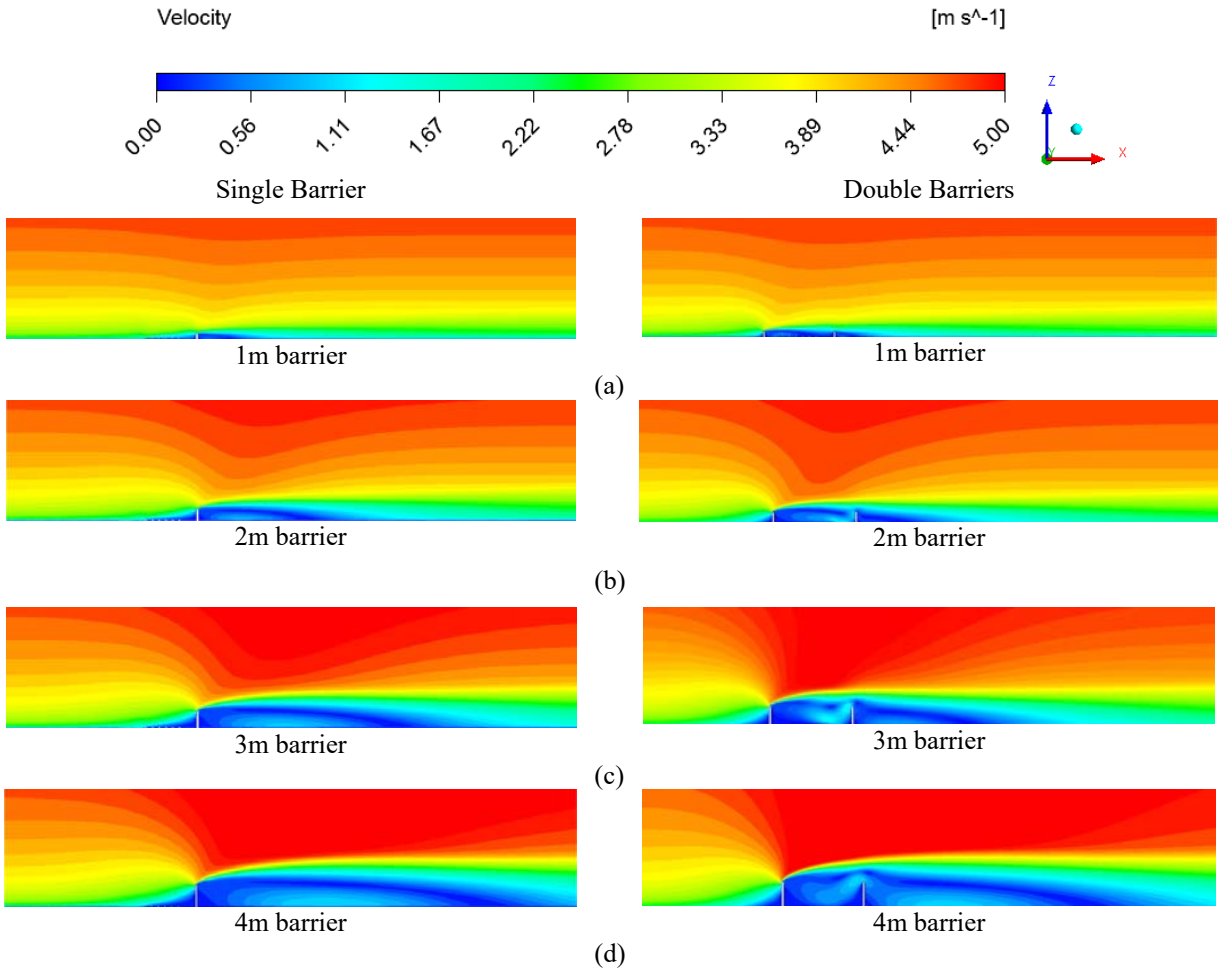

Figure 9: Velocity contour for single barrier and double barriers case with different heights at mid plane (a) 1m barrier, (b) 2m barrier, (c) 3m barrier, (d) 4m barrier

A power law velocity distribution pattern can be seen at inlet boundary. Flow experiences separation due to the existence of barriers. Wind speed accelerates near barriers top edge. The higher barrier is, the higher maximum velocity can be seen. Due to flow separation, a wake region can be formed behind downwind barriers. For double barrier case, another flow recirculation and low speed region can be seen behind upwind barrier. The higher barrier is, the bigger the size of wake region for both single and double barrier cases. With the same barrier height, single barrier case has a larger downwind wake region than double barriers cases.

Figure 10 shows the turbulence intensity distribution for both cases.

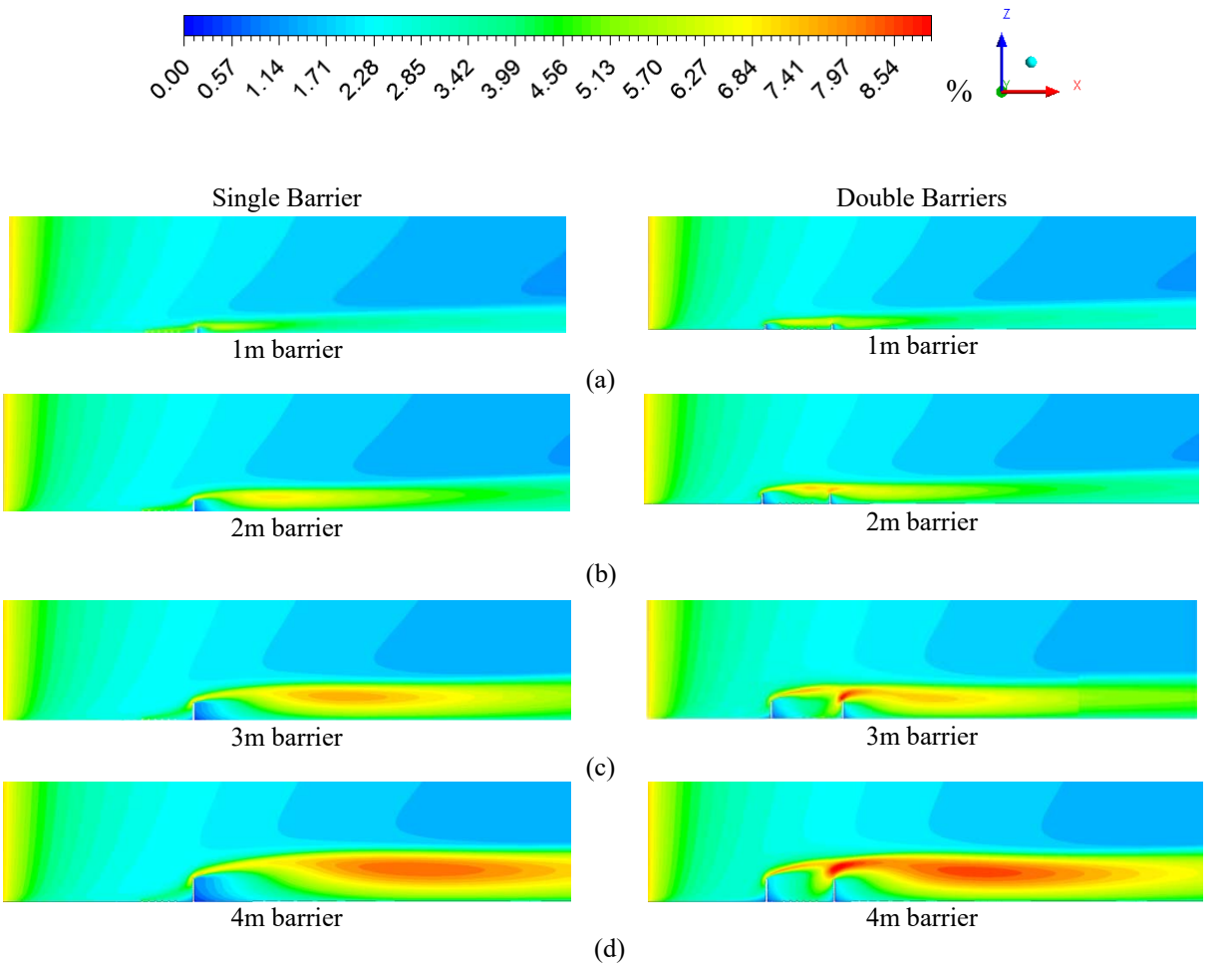

Figure 10: Turbulence intensity distributions at mid plane for single downwind barrier and double barriers (a) 1m barrier, (b) 2m barrier, (c) 3m barrier, (d) 4m barrier

Turbulence Intensity is that measurement scale. Turbulence Intensity is a scale characterizing turbulence expressed as a percent. An idealized flow of air with absolutely no fluctuations in air speed or direction would have a Turbulence Intensity value of 0%. The high turbulence intensity can be found downwind behind barriers. This happens in the wake region where the vortex generation leads flow recirculation. For both cases, the higher barrier is, the higher turbulence intensity can be seen. The area of high turbulence intensity also grows as barrier height increases. With the same barrier height, double barriers case has higher turbulence intensity downwind than single barrier case. A low turbulence intensity zone can be found behind single barrier. The size of the low turbulence intensity zone grows as barrier height increases. This cannot be found behind downwind barrier in double barrier cases.

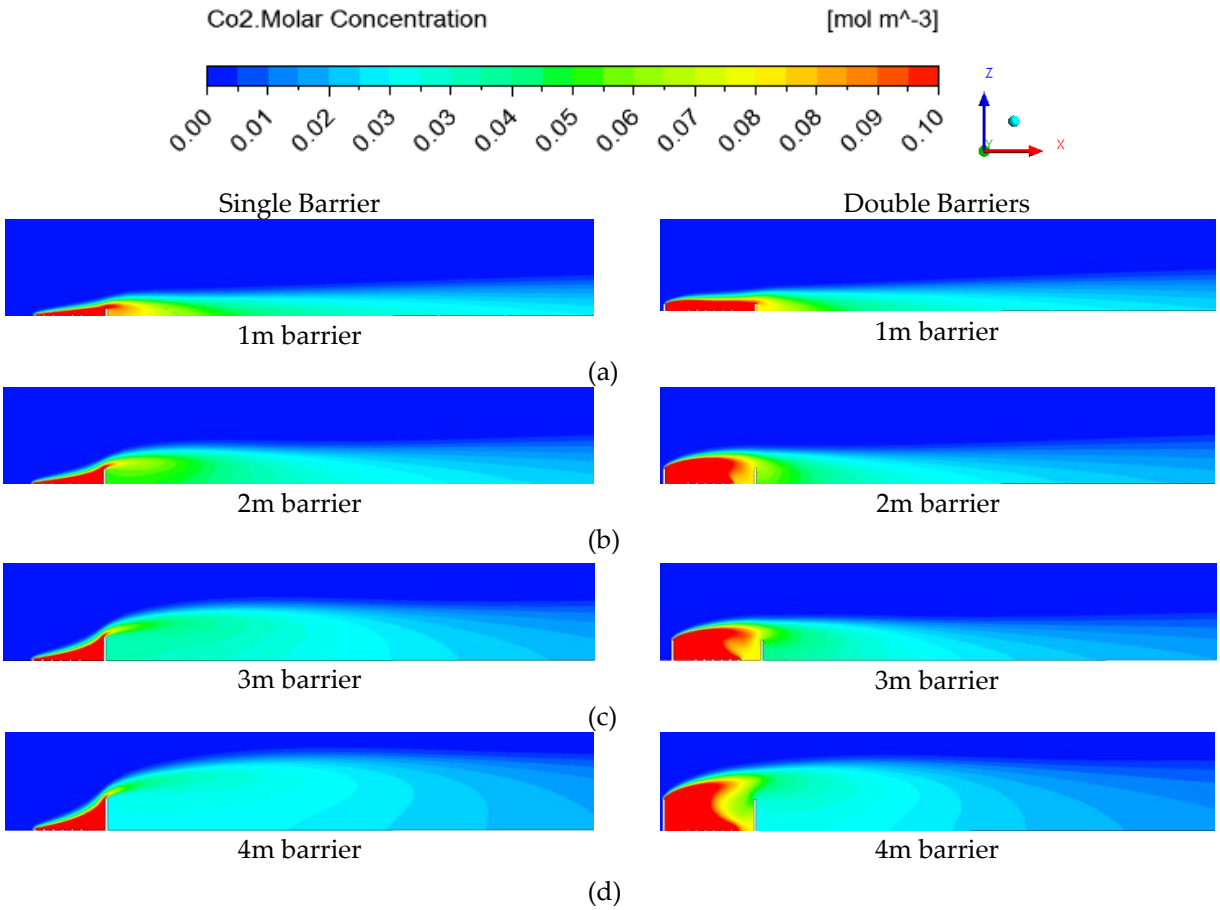

Figure 11: CO_2 concentrations at mid plane for single barrier and double barrier cases (a) 1m barrier, (b) 2m barrier, (c) 3m barrier, (d) 4m barrier

Figure 11 above shows CO_2 concentration distribution at near barriers region. For single barrier case, downwind concentration decreases as barrier height increases. The vertical span is also increased as barrier height goes up. A lift effect is done to pollutant dispersion. At the same time, a high pollutant concentration zone can be seen before barrier. For double barrier case, the same lifting effect can be seen downwind. The lifting effect increases as barrier height increases. Downwind concentration decreases as barrier height increases. With the same barrier height, double barrier case has lower concentration than single barrier case.

Figure 12 shows CO_2 concentration profile at ground level for double barrier case with different height and non-barrier case.

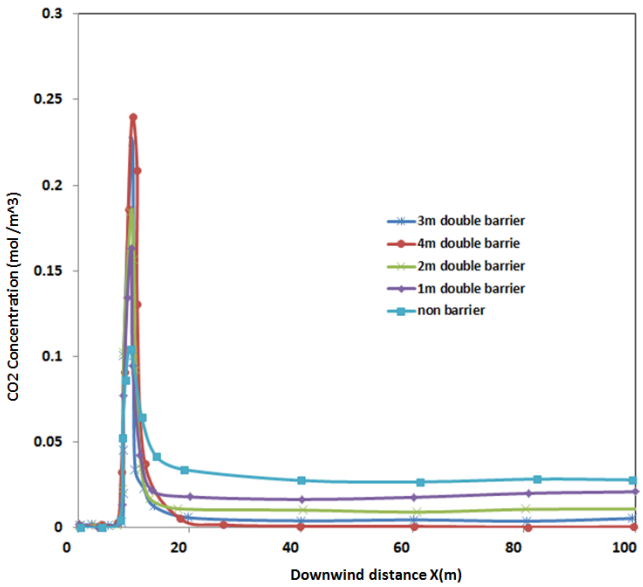

Figure 12: CO_2 concentration profile at ground level till 100m downwind for all height double barrier cases and non-barrier case

At downwind 100m, non-barrier case has a CO_2 concentration about 0.024 $^{mol}/_{m^3}$ and 4m double barrier case has concentration about 0.016 $^{mol}/_{m^3}$. It has about 80% reduction on concentration with 4m high barriers. 2m double barrier has concentration of 0.02 $^{mol}/_{m^3}$. 3m double barrier case has concentration of 0.018 $^{mol}/_{m^3}$. 1m barrier double barrier has concentration of 0.023 $^{mol}/_{m^3}$. There is about 0.002 $^{mol}/_{m^3}$ decrease on concentration with every 1m barrier height increase.

Figure 13 shows vertical concentration profile at 10m behind downwind barrier.

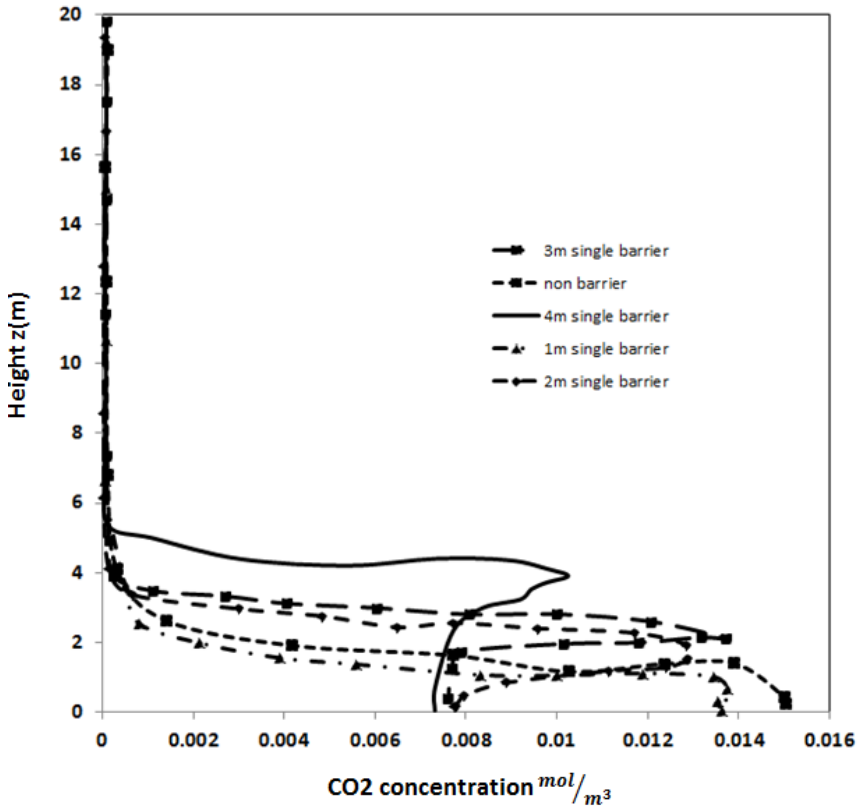

Figure 13:CO_2 concentration plots at 10m behind downwind barrier for single barrier configuration all heights

It can be seen that non-barrier case has the highest ground level concentration of near 0.0155 $^{mol}/_{m^3}$. Ground level concentration decreases as barrier height increases. The highest concentration for each barrier height can be found at the same level as barrier height. For example, highest concentration of 0.01 $^{mol}/_{m^3}$ can be seen for 4m barrier case at 4m high. 0.014 $^{mol}/_{m^3}$ can be seen for 3m barrier case at about 3m high. Concentration profile is vertically expanded due to barrier height increase. The ground level concentration can decrease to 0.0075 $^{mol}/_{m^3}$ for 4m barrier case, 52% reduction than non-barrier case.

Figure 14 shows concentration vertical profile at 10m behind downwind barrier for double barrier configuration. Similar lifting effects can be seen for all barrier heights. Double barrier has smaller concentration than single barrier case with the same height. With 4m double barrier, the

maximum concentration is about 0.0035 $^{mol}/_{m^3}$. 3m high barrier, the maximum concentration is about 0.005 $^{mol}/_{m^3}$. 2m high barrier has maximum concentration about 0.0065 $^{mol}/_{m^3}$.

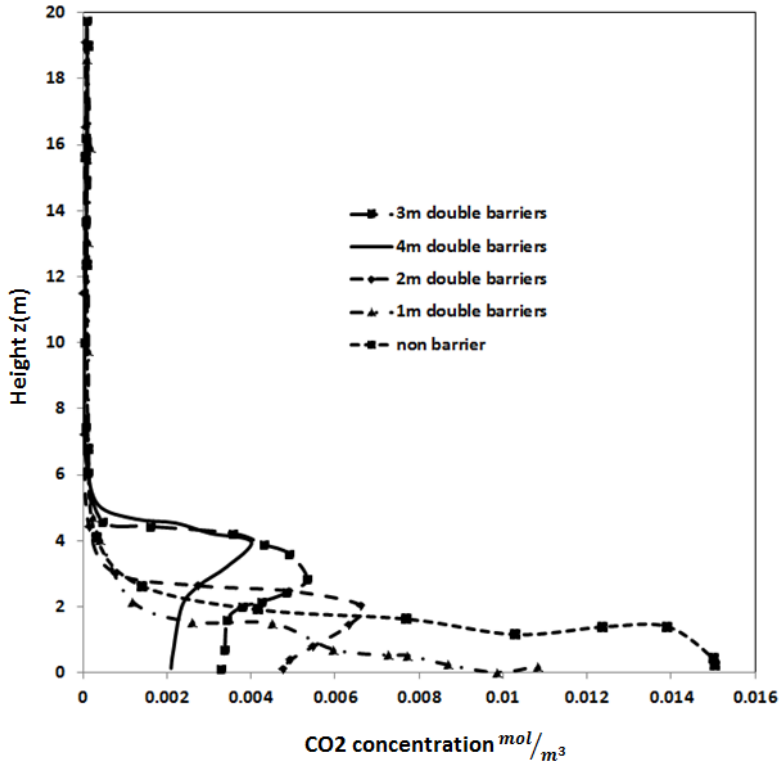

Figure 14: CO_2 concentration plots at 10m behind downwind barrier for double barriers configuration all heights

3.3 Various Thermal Stabilities Effects on Pollutant Dispersion

Study was continued by using different inlet temperature profiles to 4m single and double barriers cases. Figure 15 below shows velocity distribution results at mid plane.

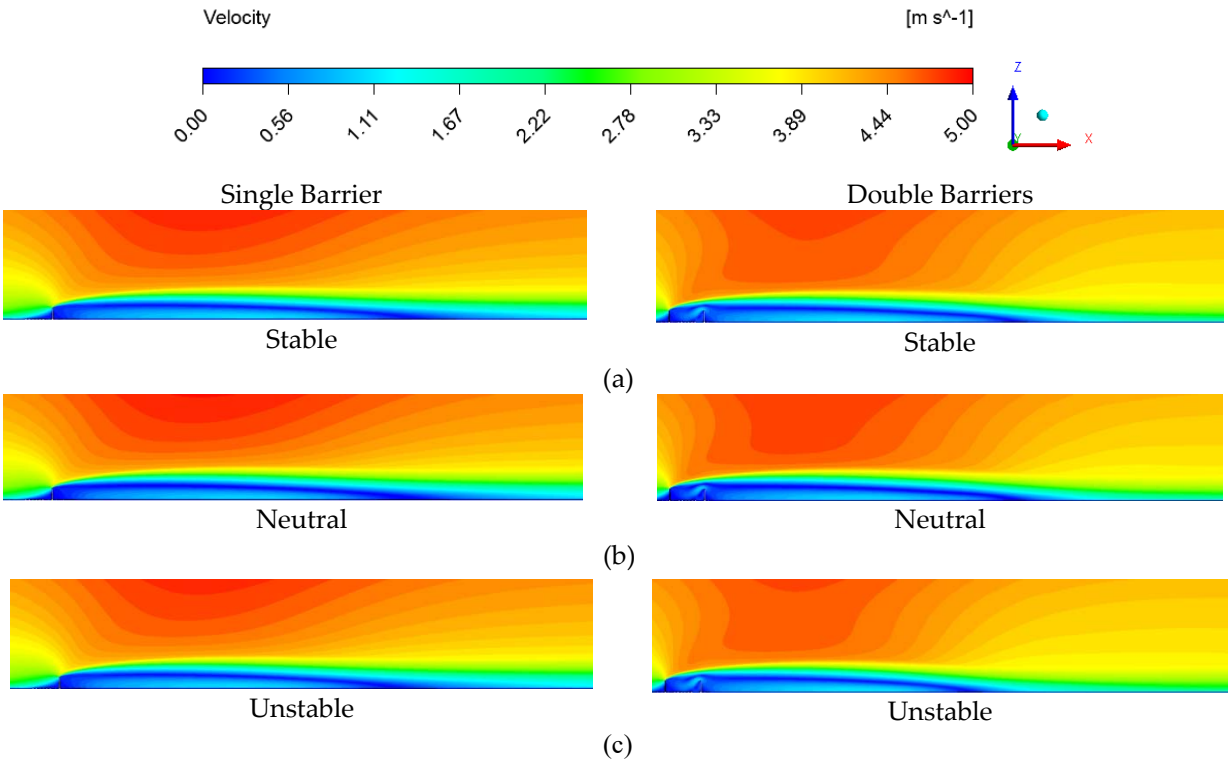

Figure 15: Velocity distributions at mid plane for single and double barrier cases at (a) Stable condition, (b) Neutral condition, (c) Unstable condition

Low speed region can be found for both cases behind barrier where the wake region located at. By observing the low speed region for three thermal conditions, unstable condition has a shorter low speed region. Stable condition has the largest horizontal span of low speed region behind barrier. Unstable condition has a faster velocity recovery behind barrier after flow separation. A faster flow speed can be found earlier in unstable case than stable case. This effect can be seen more obvious in double barrier cases. Double barrier configuration helps velocity recovery faster than single barrier case at the same thermal condition.

Figure 16 shows turbulence intensity for 4m single and double barrier cases under neutral, stable and unstable cases.

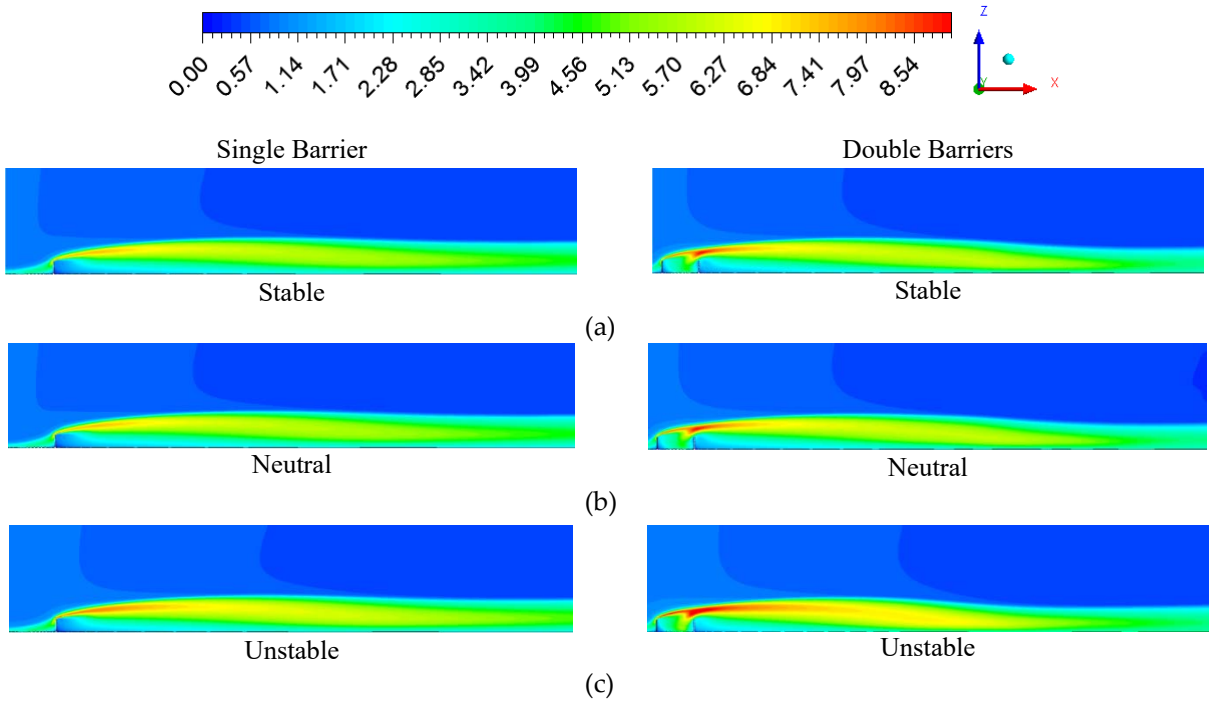

Figure 16: Turbulence intensity distributions for 4m single and double barriers cases at (a) Stable conditions, (b) Neutral conditions, (c) Unstable conditions

As described in previous section, turbulence intensity can represent turbulence level of flow. From turbulence intensity contour for single barrier cases, higher turbulence intensity can be seen for unstable condition case than stable case. Higher turbulence intensity can also be seen for double barrier cases than single barrier case at the same thermal condition. This can also explain the velocity field shown in Figure 14. Higher turbulence intensity helps turbulence mixing and induces separated flow recover faster. From the contour, the lifting effect can also be seen. Higher turbulence intensity can be found near barrier top other than ground level.

Figure 17 shows CO_2 concentration at mid plane for 4m single and double barrier cases at three thermal conditions

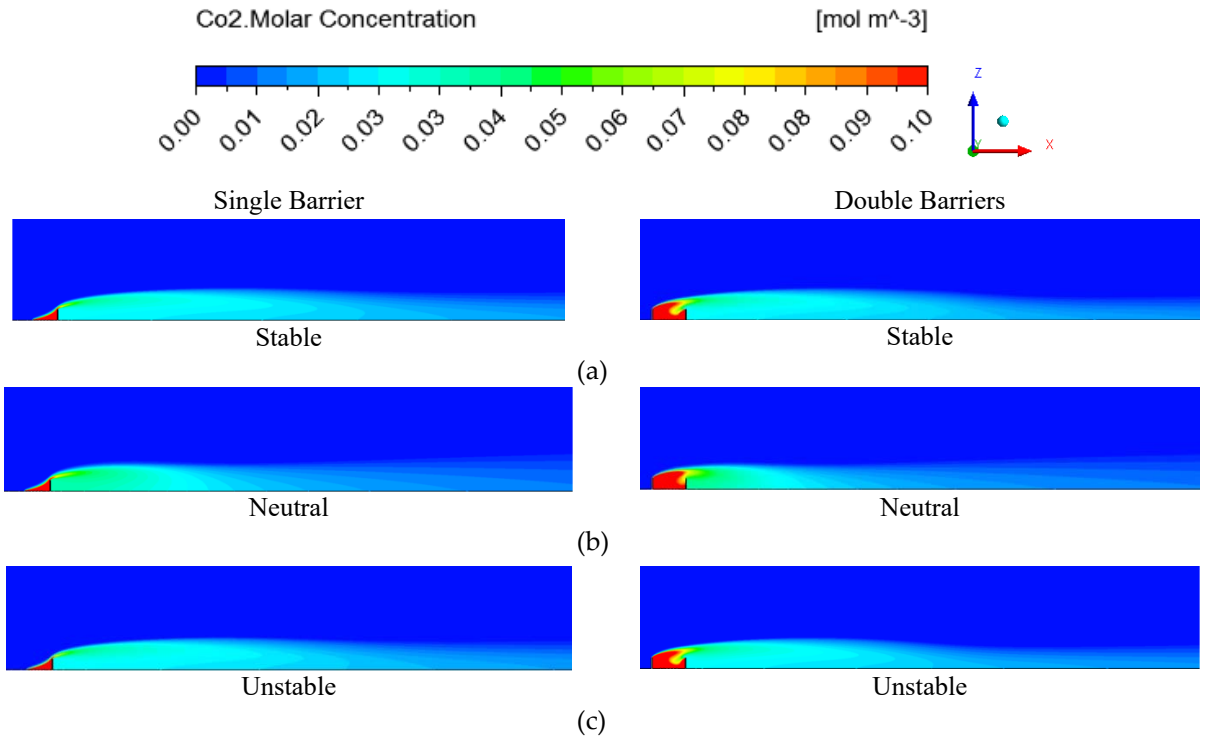

Figure 17: CO_2 concentration at mid plane for 4m single and double barrier cases at (a) Stable condition, (b) Neutral condition, (c) Unstable condition

By comparing concentration distribution for both cases, unstable condition can be seen to have the least concentration downwind behind barriers. Double barriers configuration has lower concentration than single barrier case under the same thermal condition. Very similar concentration can be seen between barriers under all thermal conditions for both configurations.

Figure 18 shows concentration vertical profile at 10m behind downwind barrier for single barrier case.

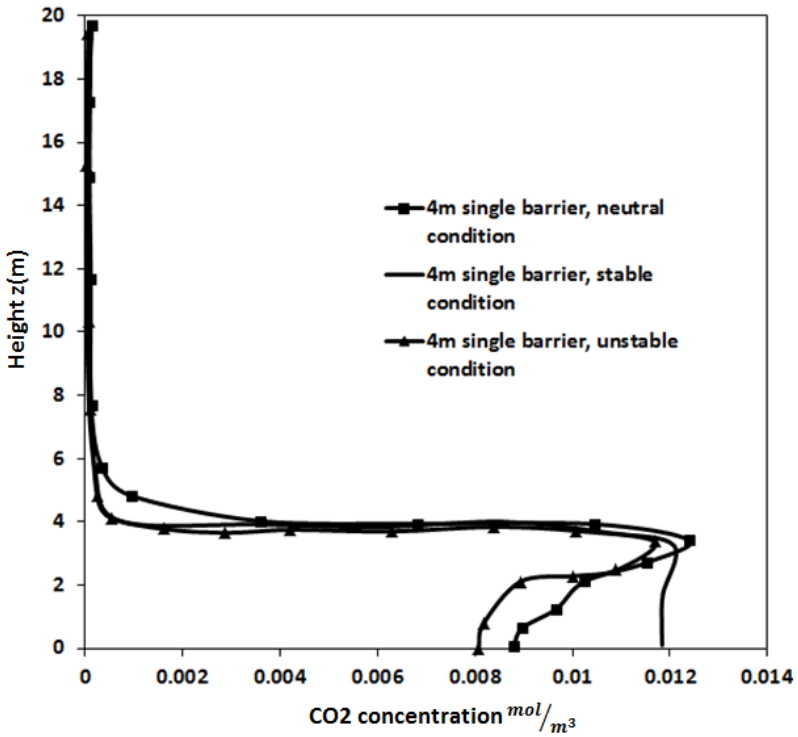

Figure 18: CO_2 concentration vertical profile at 10m behind downwind barrier for 4m single barrier under neutral, stable and unstable conditions

Unstable condition has the least ground level concentration for all the cases. In figure 18, concentration vertical profiles were plotted at the same barrier height under three thermal conditions. It can be seen that the maximum concentration are almost the same for all conditions. The location of maximum concentration is near barrier edge for all cases. Stable condition has similar concentration values for height below 4m. Neutral condition has smaller concentration for height below 4m. Unstable condition has smaller concentration for height below 4m as well. Concentration decreases as the height gets closer to ground level. This is due to lifting effect. Stable condition does not have a big lifting effect. Pollutant distributes uniformly in vertical direction.

3.4 Summary of Results

In this section, simulations were done to two noise barriers configurations: single downwind barrier and double barriers. Study was focused on barrier height effects and thermal effects. Studied heights are 1m, 2m, 3m, and 4m. Various thermal conditions were modeled by different inlet temperature profiles.

It proved that noise barrier helps reduce downwind pollutant concentration for both configurations. However, double barrier case has lowest downwind concentration at the same barriers height case. The reduction in concentration increases as barrier height increases. This corresponds to the faster velocity, smaller wake region behind barrier, high turbulence intensity. Double barriers also have relatively high pollutant concentration between barriers. Pollutant gets trapped between barriers.

As of thermal effect, it was found that unstable condition tends to have the least concentration than stable and neutral conditions. Faster velocity behind barrier and high turbulence intensity can be found for unstable condition case. It was found high turbulence intensity helps faster turbulence mixing and flow recovery. Therefore, unstable condition has a lower concentration downwind.

At the same thermal and height, double barrier configuration has better concentration reduction effects than downwind single barrier configuration. Unstable condition helps pollutant disperse faster and has a lower ground level pollutant concentration.

4. NOISE BARRIER SIDE EDGE EFFECTS ON POLLUTANT DISPERSION

4.1 Problem Description

Noise barrier edge effect was first mentioned in 2013 by Steffen et al. Barrier edge effect happens with relatively shorter noise barriers configurations along road. The vertical side edges of barriers could separate flow and induce flow recirculation. Sensitivity study of wind angle and wind speed on effect of barriers edge effect was carried. It described that edge effect might cause secondary recirculation and came up with conclusion that edge effect gets stronger with higher wind speed. However, there were no further detailed analyses of results on noise barrier edge effects on pollutant dispersion and no further studies about thermal effects either.

The purpose of this study is to analyze barriers edge and atmospheric boundary layer effects on flow field and pollutants dispersion near roadside. Simulation will be done to double barriers configuration with different heights. Study barriers length is 50 meters. Total domain width is 200 meters. Figure 19 shows computational domains for two configurations. Results will provide valuable input to roadside barriers design and improve the roadside air quality.

Turbulence flow modeling, wind inlet profile and different thermal boundary conditions used will be the same as previous section.

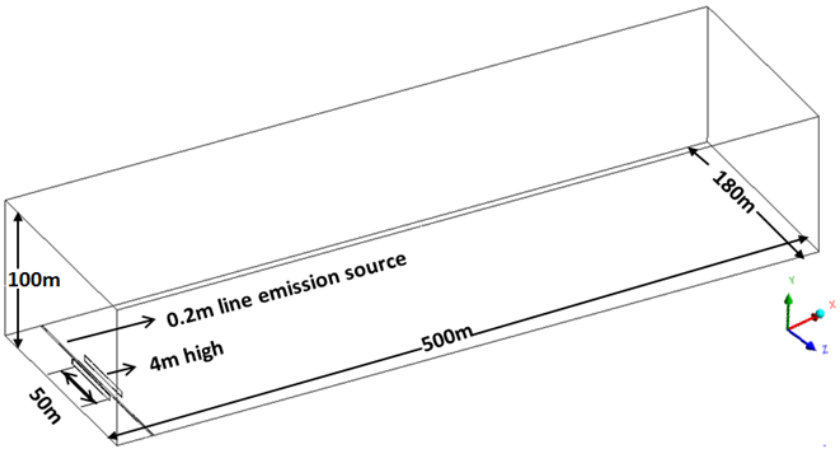

(a) With edge effects double barriers computational domain

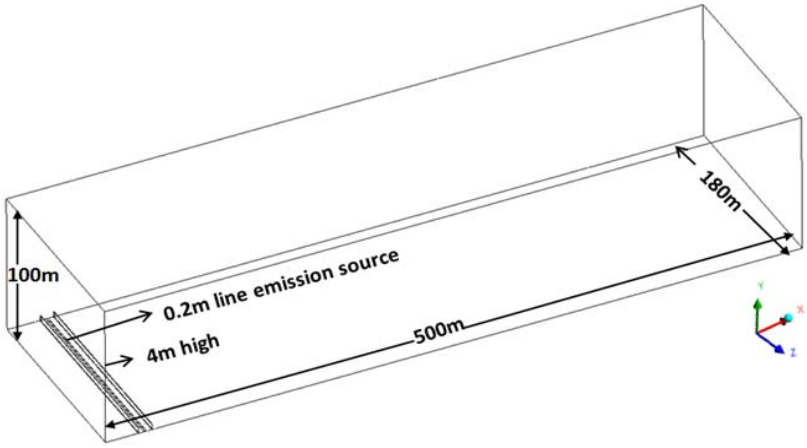

(b) Without edge effects double barriers computational domain
Figure 19: Computational Domain for Edge Effects Study

4.2 Noise Barrier with Edge Effects under Neutral Conditions

4.2.1. Flow characteristics comparison between edge effect and non-edge effect

In this section, simulation results of flow characteristics such as velocity, turbulence intensity and turbulence kinetic energy (TKE) are compared between barriers with and without edge effect geometries with various barriers height under neutral condition in order to show how the existence of barrier edges influence flow field.

Figure 20 shows velocity magnitude streamline in the middle iso-surface (Y=250m). Plotted area has a 100 meters horizontal span in X axis direction and 10 meters vertical height in Z axis direction

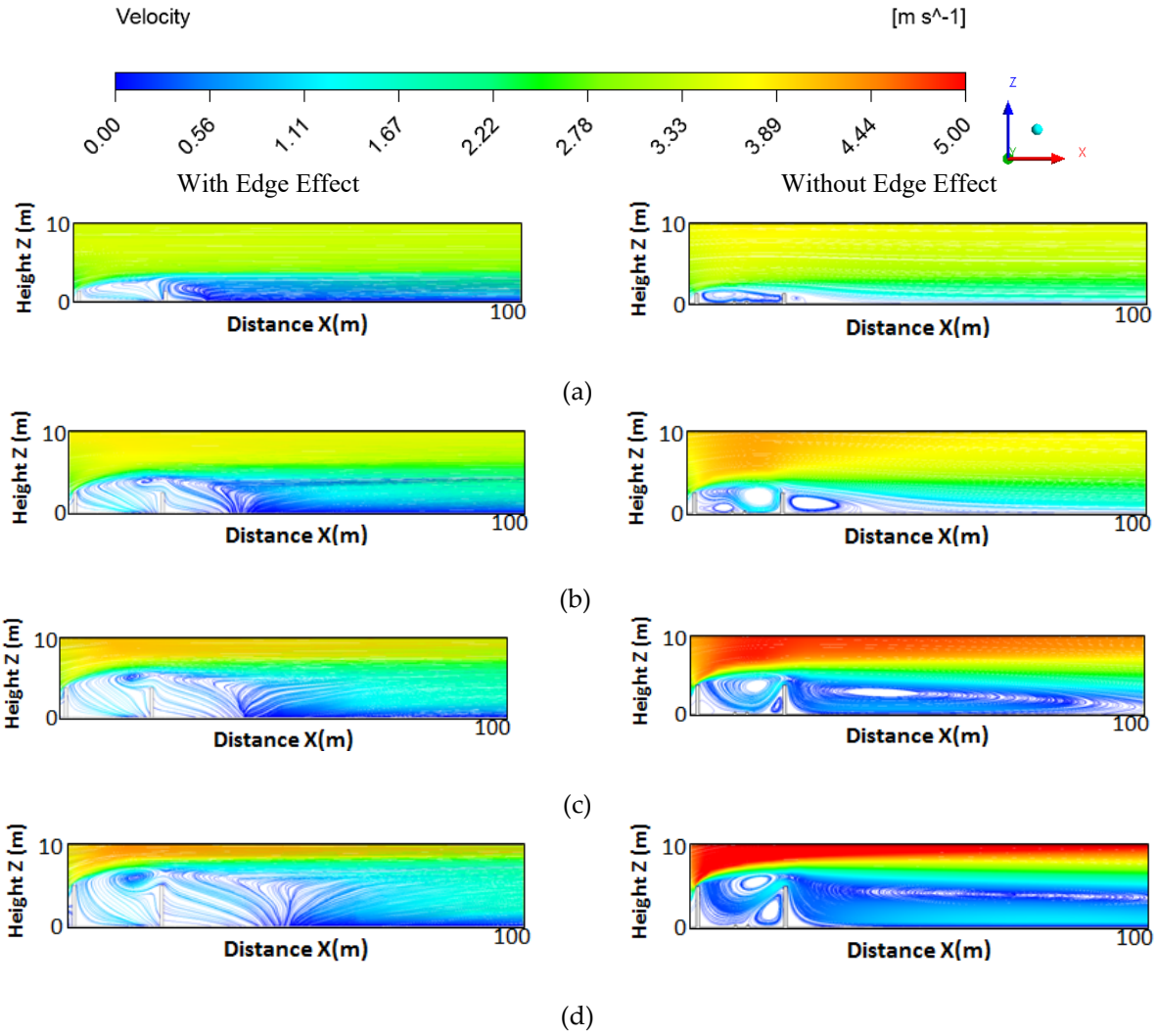

Figure 20: Comparison of streamline in symmetry plane (Y=250m) for barrier geometry with and without edge effects at different barrier heights under neutral condition. The noise barrier height is (a) 1m (b) 2m (c) 3m and (d) 4 m.

As shown in Figure 20, velocity starts to accelerate on the top of upwind barriers. This is a low speed zone is formed between barriers. Velocity starts to decelerate as the wind passes downwind barrier and tends to recover further downwind. The maximum velocity increases as barriers height increases. The behavior of flow velocity induced negative pressure zone between barrier and behind downwind barrier. A wake region is formed, where has a low speed, pressure and high turbulence level flow recirculation. Due to the existence of flow recirculation, the flow field of non-edge effect barrier geometry has vortices regions generated in between barriers and behind downwind barrier. In between barriers, multiple vortex regions can be generated as barrier height increases. A second vortex near the bottom of barriers can be seen grow bigger as the barriers height increases. The center of the first generated vortex region located on the top can be seen lifted up as barriers height increases. Similarly a wake region of vortices is formed behind downwind barrier. The size of the wake region can be seen grows bigger as barrier height increases. The center of the wake is shifted further away from barrier horizontally as barrier height increases.

For edge effect case, only one vortex region can be seen near the top of downwind barrier. It can also be noticed that the size of the vortex increase as barrier height increases. No complete vortex region can be found behind downwind barrier. This is caused by the mixing of barrier side edges induced flow and top edge induced flow. Velocity magnitude is smaller than non-side edge barriers at the same barrier height.

Figure 21 shows another group of streamline profiles for two barrier geometries. However, the plotted surface is 10 meters away from middle plane in Y direction (Y=240m). A great similarity of velocity distribution can be seen for non-side edge effect cases. It shows that velocity distribution maintains the same in lateral span of entire computational domain (Y-direction) without considering barrier side edge effects. However, we can see different flow pattern for cases with side edge effects at plane Y=240m. A complete single vortex is formed between barriers. In area behind downwind barrier, a complete recirculation zone can also be noticed to form. Middle plane Y=250m is the symmetry plane of the computational domain and barrier geometry. Flow pattern within symmetry plane varies from non-symmetry plane.

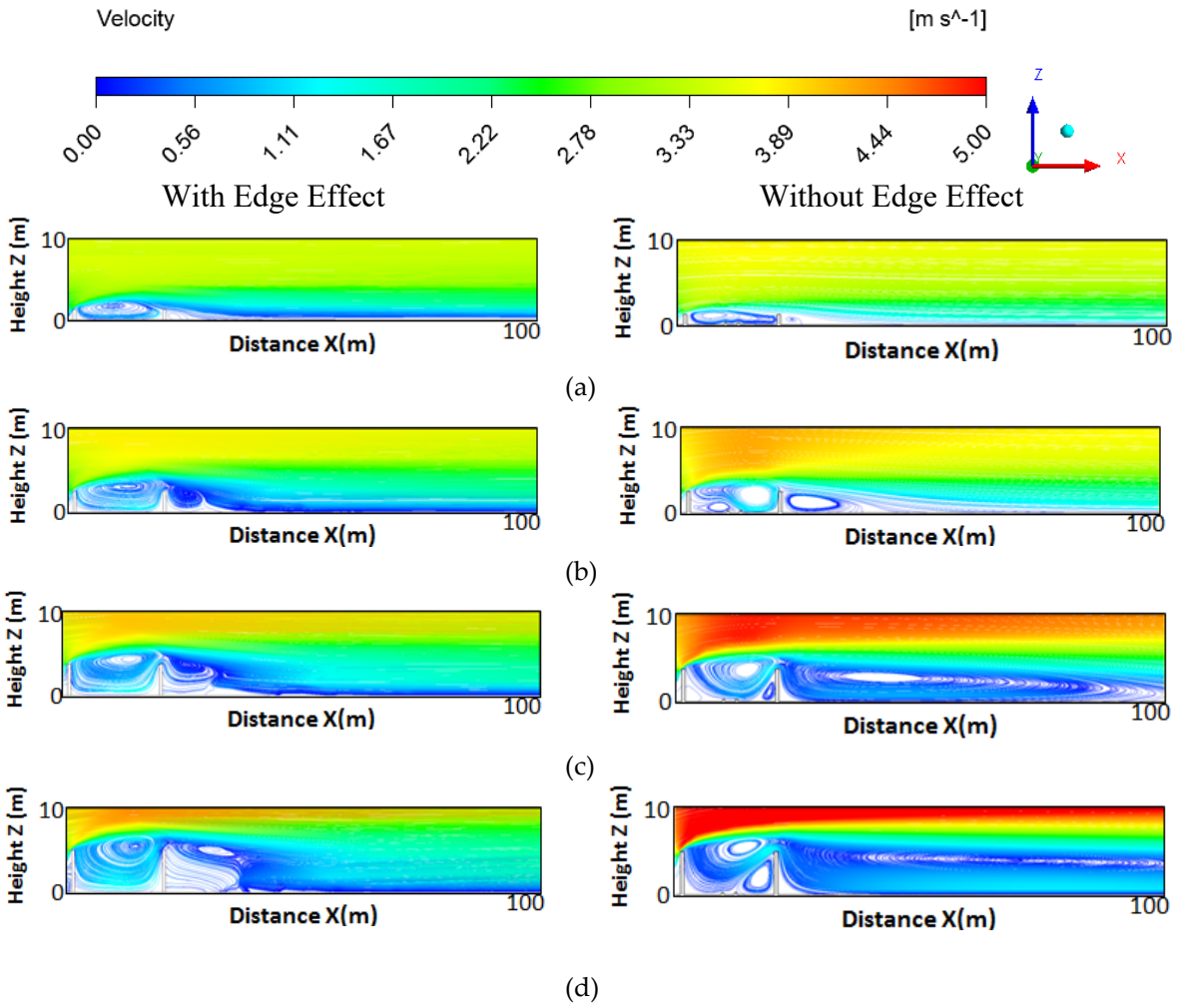

Figure 21: Streamline at plane Y=240m(10 meters away from symmetry plane) for comparing effects of barrier geometry with and without side edges under neutral condition. The noise barrier height is (a) 1m (b) 2m (c) 3m and (d) 4 m.

Figure 22 is contour plots of turbulence intensity distribution. Figure 22 shows contour of turbulence intensity in the middle symmetry plane for both with and without side edge effect cases, while For barriers with side edges introduced, turbulence intensity distribution in symmetry plane differs from non-symmetry plane. Higher turbulence intensity tends to appear in symmetry plane for barriers with side edges effects than non-symmetry plane. The maximum turbulence intensity for all conditions tends to locate near top of the downwind barrier. Lower turbulence intensity can be found near barrier bottom. Also, without barrier side edge cases have relatively smaller turbulence intensity downwind for all barrier heights. However, higher turbulence intensity between barriers can be seen for with side edge condition rather than for non-side edge conditions.

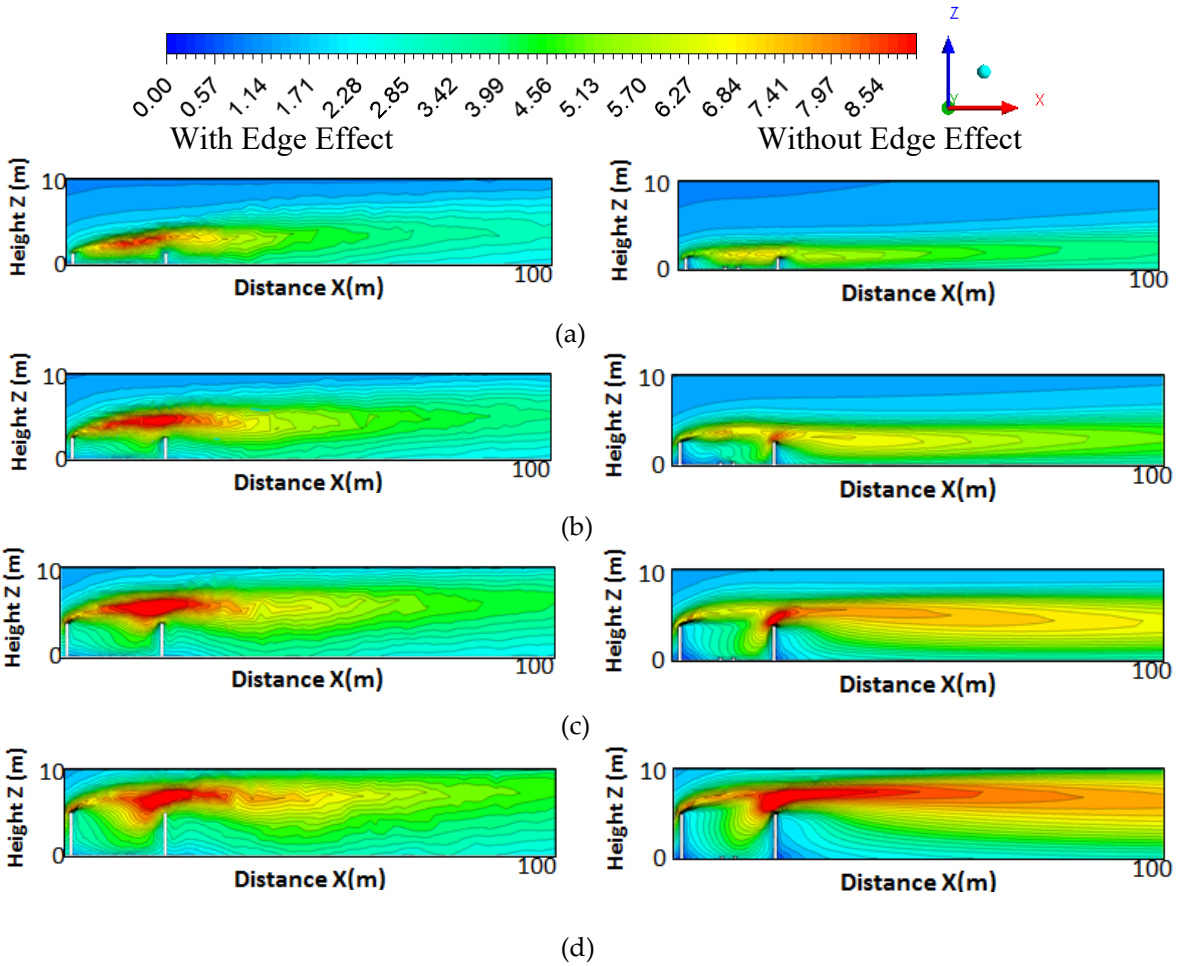

Figure 22: Contour of turbulence intensity at plane Y=240 (10 meters away from symmetry plane) for comparing effects of barrier with and without side edges under neutral condition. The noise barrier height is (a) 1m (b) 2m (c) 3m and (d) 4 m

Figure 23 is vertical profile of turbulence kinetic energy in the symmetry plane (Y = 90m) at X = 100m for with and without side edges cases. For both cases, peak turbulence kinetic energy value increases as barriers height increases. However, for barriers with edge effects at the same height level, the turbulence kinetic energy is higher. The biggest difference is 36% for 1m barrier height case.

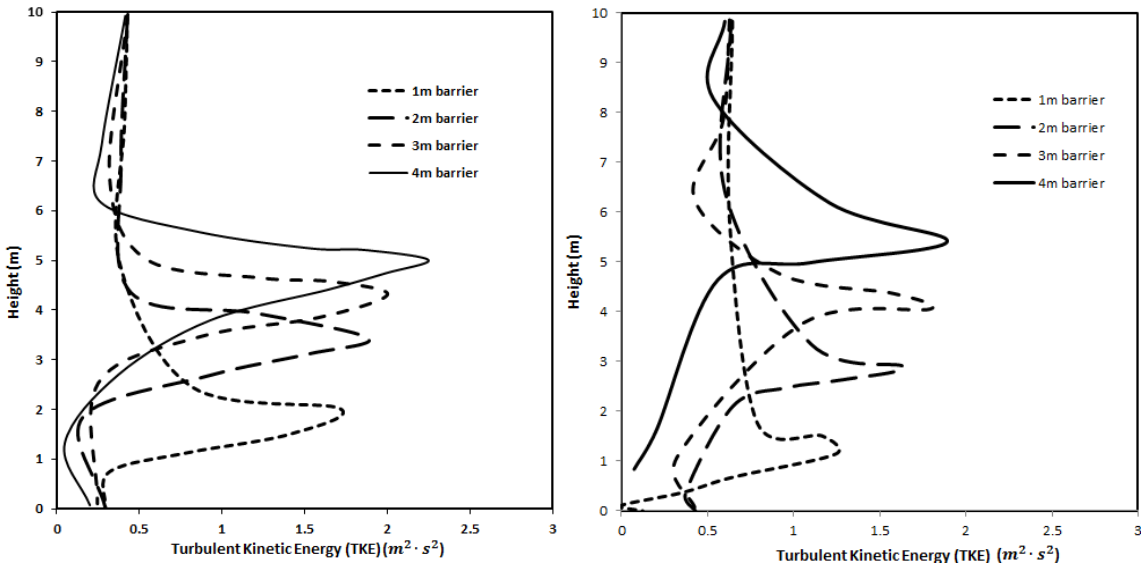

(a) (b)

Figure 23: (a) Turbulence kinetic energy vertical profile in the symmetry plane for barriers with side edges. (b) Turbulence kinetic energy vertical profile in the symmetry plane for barriers without side edges.

Table 2: Comparison of the Peak value for turbulence kinetic energy in the symmetry plane for barriers with and without edge effects cases

TKE $(m^2 \cdot S^{-2})$ / Barrier height (m)	Barrier with edge effects	Barrier without edge effects
1	1.70	1.25
2	1.96	1.56
3	2.00	1.86
4	2.30	1.98

4.2.2. Concentration comparison between edge and non-edge effect

In the previous section, we discovered how flow characteristics are affected by the existence of barrier side edges downwind and in between noise barriers. Comparing with non- side edges effects barrier configuration, flow characteristics distribution along Y direction is not always the same across the entire domain due to the mixing of multidirectional flow induced by barriers top edge and side edges. Turbulence intensity can be represented by turbulence kinetic energy of the flow. Turbulence kinetic energy is a buoyancy produced term that is directly determined by advections and dissipation rate. The concentration of a passive pollutant is determined by the horizontal advection, vertical advection, horizontal diffusion, vertical diffusion, and source or sink of pollutants. That being said, pollutant dispersion is affected by flow field. In this section,

we will discuss the effects of flow field on pollutant dispersion and barriers edge effect on pollutant dispersion.

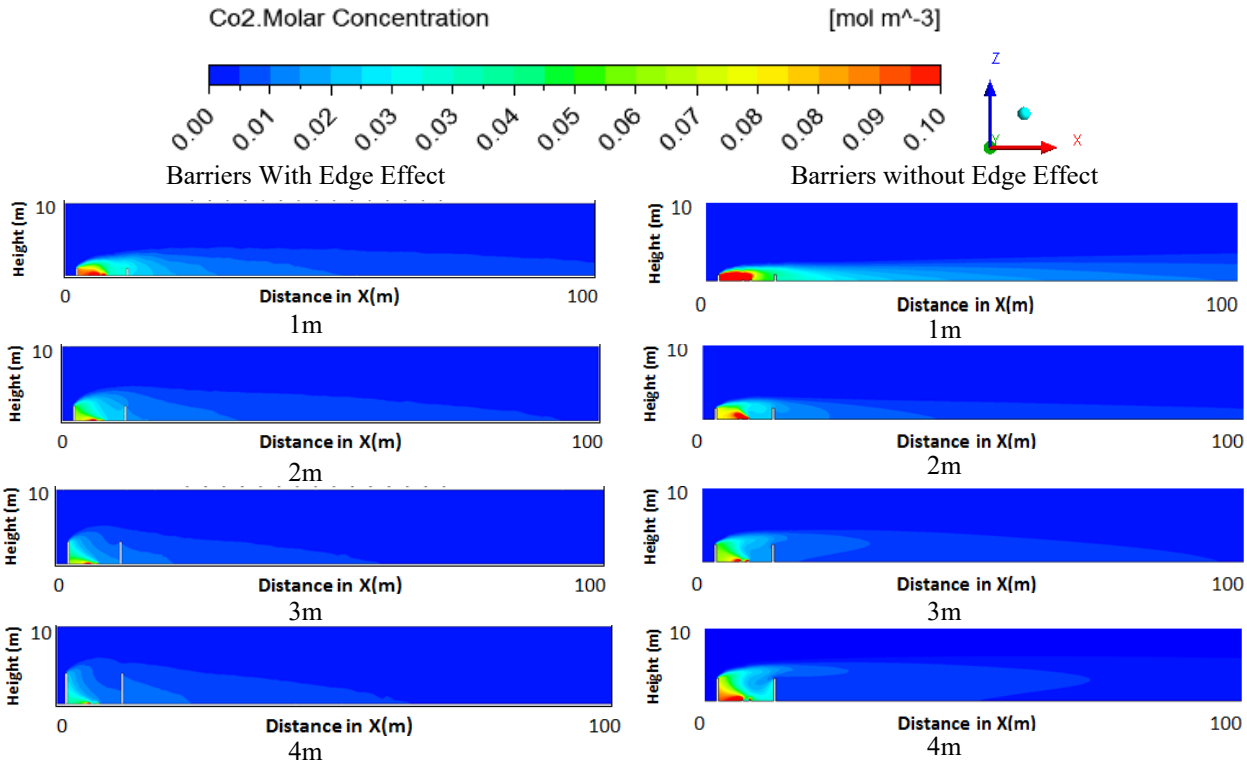

Figure 24: CO_2 Concentration at different downwind distances within 10m height

Figure 24 shows contour of pollutant dispersion in symmetry plane. A difference in downwind concentration can be seen for with and without edge effects cases. Higher pollutant concentration can be found in downwind locations for with side edge effect cases than non-side edge effect cases. In the area between barriers, with side edge cases have less pollutant concentration than non-side edge cases. This pattern follows turbulence intensity profiles shown previously in Figure 22 and velocity magnitude streamline plotted in Figure 21. Higher turbulence intensity between barriers and lower turbulence intensity downwind can be found for wide side edge effect cases than non-side edge effects with all barrier heights. Wind speed and turbulence intensity determines turbulent mixing and flow intensity. This will directly affect pollutant dispersion. Higher turbulence intensity and wind speed help pollutant dispersion faster.

Figure 25 shows CO_2 concentration contour in X-Y plane (partial top view) at ground level (z=1).

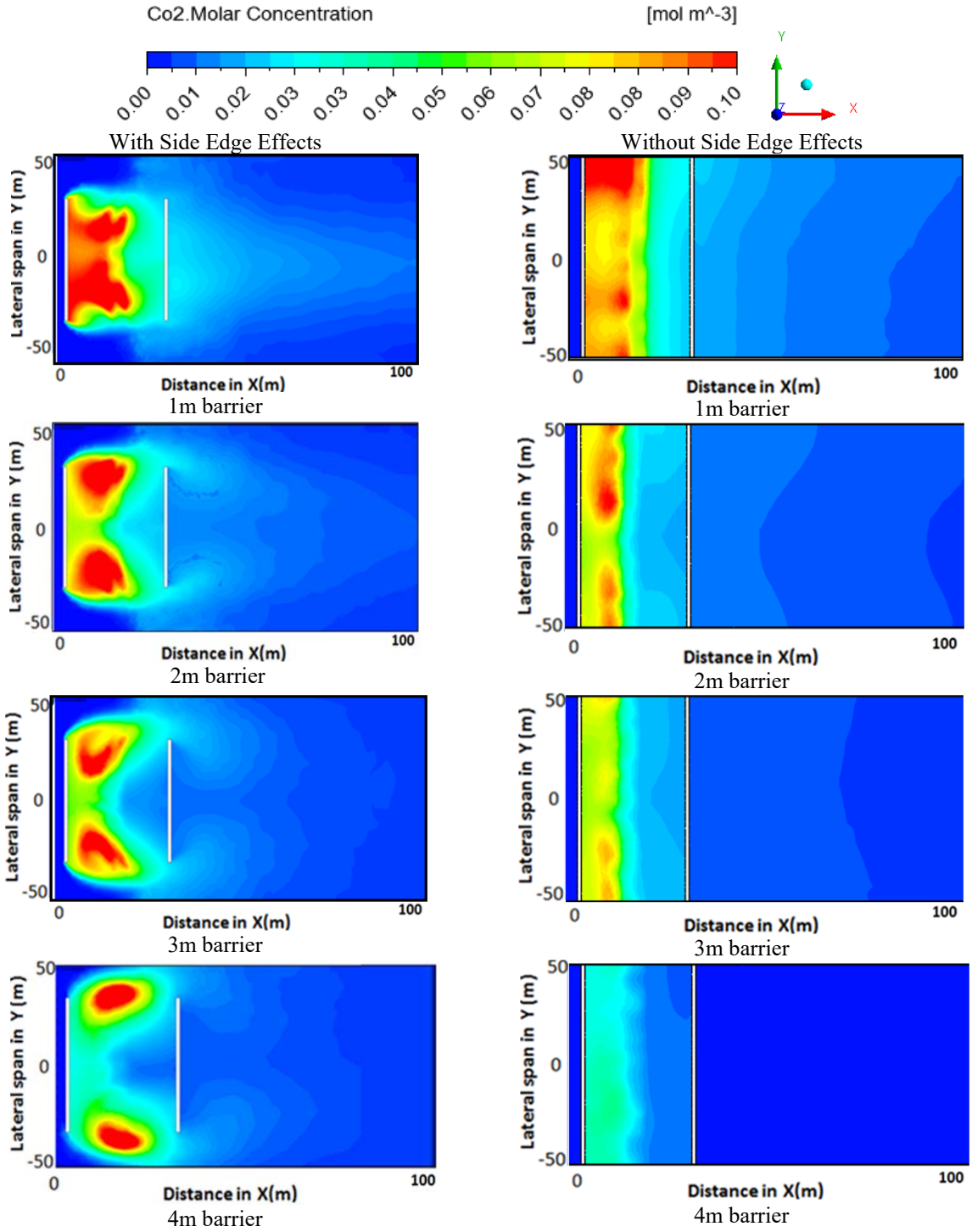

Figure 25: CO_2 Concentration for with and without side edge effects cases in X-Y plane

Figure 25 gives a clear look at concentration distribution for on road region between barriers and downwind behind barriers. High concentration zones can be seen between barriers due to pollutant trapped by flow recirculation. For 2m, 3m and 4m barrier with side edge effects cases, high concentration regions are separated into two zones, high concentration region between

barriers for 1m barrier height does not get separated. It can be seen that side edges do not show apparent effects on 1m barrier height case. Side edge impact increases as barrier height increases. This concentration distribution pattern follows the flow field distribution pattern between barriers introduced in the previous section. The highest concentration can be found at the vortex center.

Comparing concentration for cases with side edge effects and non-side edge effect at the same barrier height, the prior ones have less concentration between barriers and higher concentration downwind behind barriers. For non-side edge cases, it can be seen that high concentration happens near upwind barrier for non-side edge effect cases at all heights. Highest pollutant concentration decreases as barrier height increases. There is no accumulated separate high concentration regions can be seen between barriers. It has relatively uniform concentration distribution between barriers and downwind.

Figure 26 depicts concentration profile right behind downwind barrier (10m) for edge effect cases. Contaminant concentration decreases as the height of the noise barrier increase. Most profiles do not follow Gaussian shape distribution. However, with 1m barrier, concentration near barrier shows similar shape as Gaussian distribution. The concentration profile near barrier is strongly affected by edge effects, and those effects increase as the height of noise barrier increase.

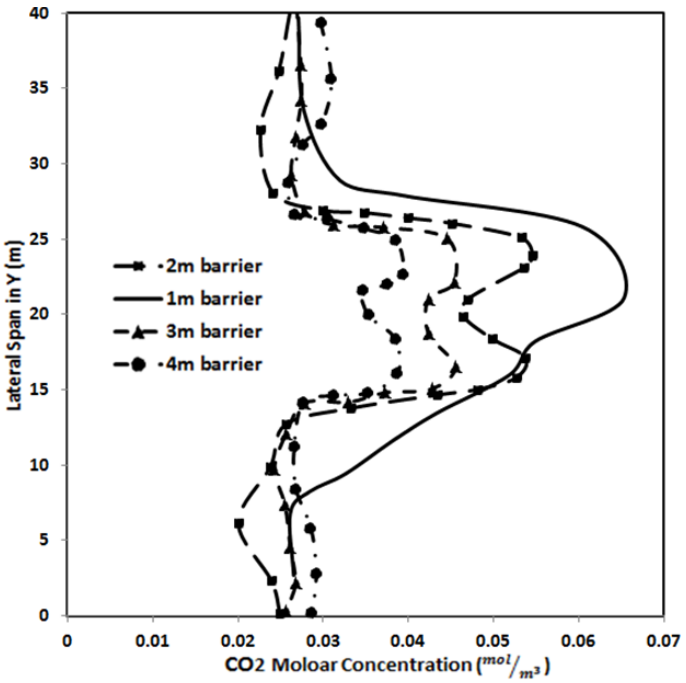

Figure 26: CO_2 concentration profile at downwind X = 10m

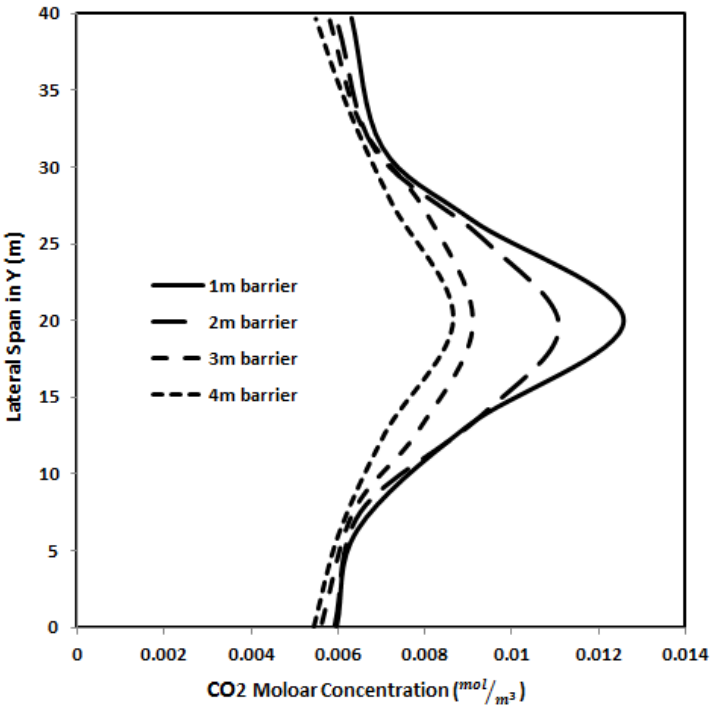

(a) with edge effect cases

Figure 27: CO_2 concentration lateral profile for without side edge effect cases at downwind x=100m (a) with edge effect cases (b) without edge effect cases

Figure 27 Continued

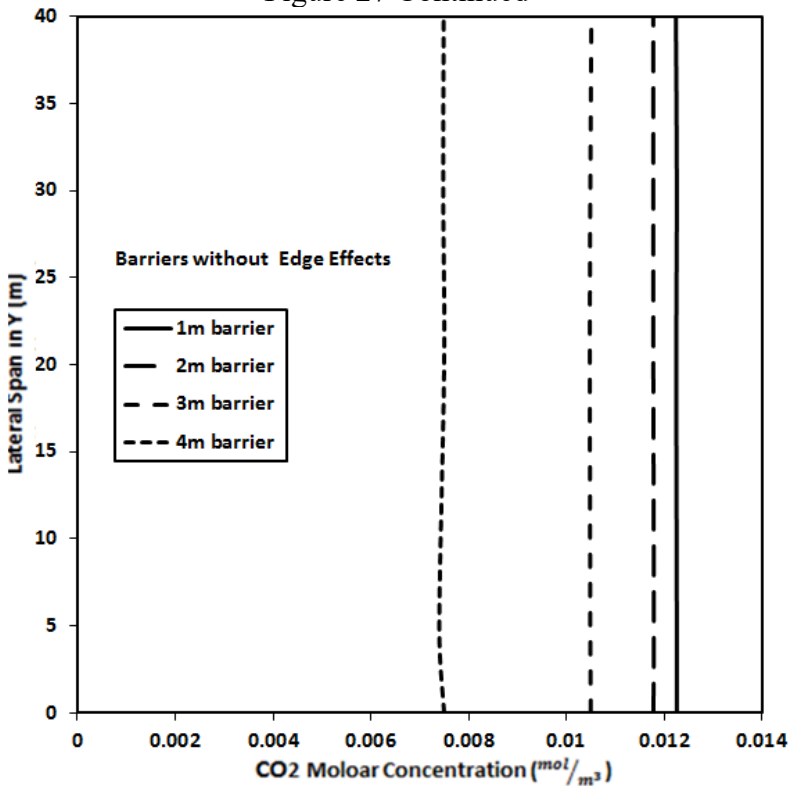

(b) without edge effect cases

At further downwind location X = 100m, with different barrier height, CO_2 concentration profiles are shown in Figure 27. For edge effect cases, all the concentration profiles at different barrier heights follow a similar shape as Gaussian distribution. A peak concentration can be found for all barrier heights at the symmetry plane. Peak concentration value decreases as the barrier height increases. 1m barrier case has the maximum peak concentration about 0.014 mol⁄m^3 and 4m barrier case has the minimum peak concentration about 0.009mol⁄m^3. Figure 14 (b) shows CO_2concentration profiles with different barrier height for without edge effect cases. An almost uniform distribution of CO_2 concentration can be observed.

The concentration deficit region behind downwind barrier can be seen as a wake region induced by flow separation. In order to verify the concentration distribution in wake region follows Gaussian shape pattern, a self-similar concentration-deficit profile against normalized radial distance from the center of the wake (l/l(1⁄2)) was plotted the same way as described in Abkar et

al. For downwind location x satisfies x/W >4, the self-similar concentration deficit profile is expected to collapse into a single Gaussian curve except at the edge of the wake [21]. X axis is l/l, l(1/2)is half of wake width. Vertical Y axis is normalized concentration ΔC/(ΔCmax). Results show that at different downwind locations for the same barrier height case, concentration deficit follows a single Gaussian shape distribution as shown in the Figure 28. This validated the self-similar Gaussian shape of concentration deficit at certain downwind locations. It can be seen that, for different barrier heights, the Gaussian curve follows the same trend for the two downwind locations X/H=4 and X/H=6. H is barrier height.

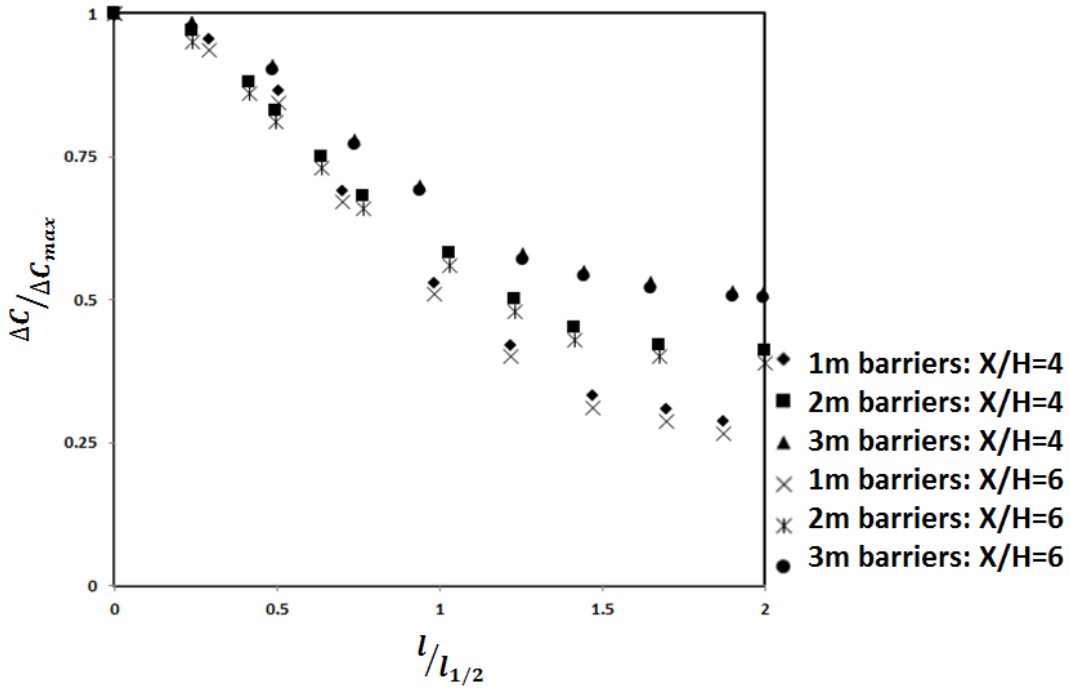

Figure 28: Self-similar pollutant concentration deficit profiles at different downwind locations at different barrier height.

4.2.3. Noise barriers with edge effect under stable and unstable thermal conditions

Figure 29 shows concentration contours at various barrier heights under different thermal stability conditions for with side edge effects cases.

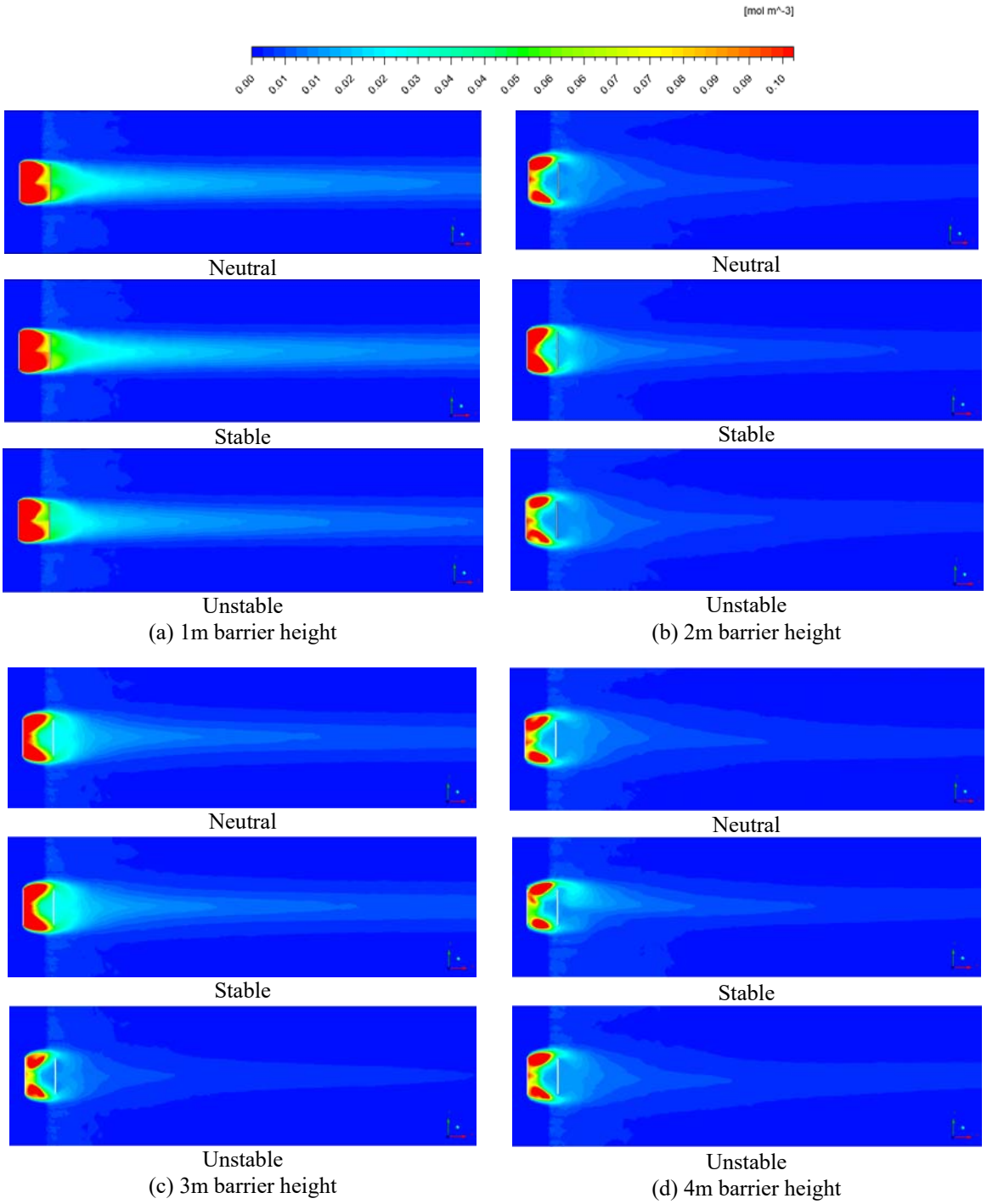

Figure 29: Ground level (Z = 1 m) CO_2 concentration for both with and without edge effects under various thermal conditions for various noise barrier heights (a) 1m barrier; (b) 2m barrier ;(c) 3m barrier ;(d) 4m barrier.

Results show that, unstable condition has the least concentration at all barrier heights. Stable condition has the highest concentration. Unstable condition has stronger turbulence mixing effect on flow field downwind. This leads to a faster flow velocity recovery on separated flow which

leads to faster pollutant dispersion. As the noise barrier height increase, the pollutant disperses distance decreases. In the area between barriers, high concentration area can be seen separated into two regions due to edge effect as barrier height increases. At 1m barrier height, the high concentration region is not separated. As barrier height increases, edge effects get stronger.

4.3.Summary of Results

This study was done to study barriers side edge effects with multiple barrier heights and various atmospheric thermal boundary conditions. Numerical models were first validated with experimental and theoretical data. Second, simulations were conducted which were focused on neutral condition to study how barrier side edges affect flow properties such as velocity, turbulence intensity and turbulence intensity in flow field. Third, the effects on the pollutant concentration distributions from different atmospheric thermal conditions (neutral, stable and unstable).

To consider the concentration distribution, two regions are analyzed: area between barriers and downwind behind barriers. In the area between barriers, higher velocity magnitude and turbulence intensity can be found for cases with side edge cases. This explains the less pollutant dispersion seen with side edge cases. In downwind area, higher velocity and turbulence intensity can be found for non-side edge effect cases. Therefore, less downwind pollutant concentration can be noticed for non-side edge effect cases. Concentration decreases as barriers height increases for both cases. With 1m barrier, side edge impact is not strong to separate flow between barriers.

Considering the different thermal boundary effects, it was found that unstable condition causes the least downwind concentration and stable condition results the highest downwind concentration with the same barrier height. Concentration profiles between barriers are similar for all three thermal conditions. However, downwind concentration profile shows big difference for different thermal conditions.

Overall barriers feature can help reduce downwind pollutant concentration. Non-side edge effect cases tend to have higher pollutant concentration on road between double barriers; this can be solved by introducing proper side edge with a certain height.

5. NOISE BARRIERS EDGE EFFECTS UNDER OBLIQUE WIND PROFILES UNDER DIFFERENT THERMAL CONDITIONS

5.1 Problem Definition

In Steffens et al. 2013, barrier edge effect was first introduced. It also concluded that edge effects get stronger with oblique wind relative to barriers. In this section, simulation was done to three different angles of wind inlet profile to study oblique wind angle effect on pollutant dispersion.

The distance from inlet to emission source maintained to be 25m. Distance between downwind single barrier to nearest lane is 3.5m. Oblique wind profile is simulated by tilting barrier and source geometry to certain degree. Three angles were studied. The first case is 90° angle, wind profile is perpendicular to road lanes and barrier. The second case is oblique wind, the angle between wind direction and horizontal direction is 75°. The third case is oblique wind with angle of 60°. Figure 30 shows computational domain of three wind conditions. Barrier height is 4m in this study.

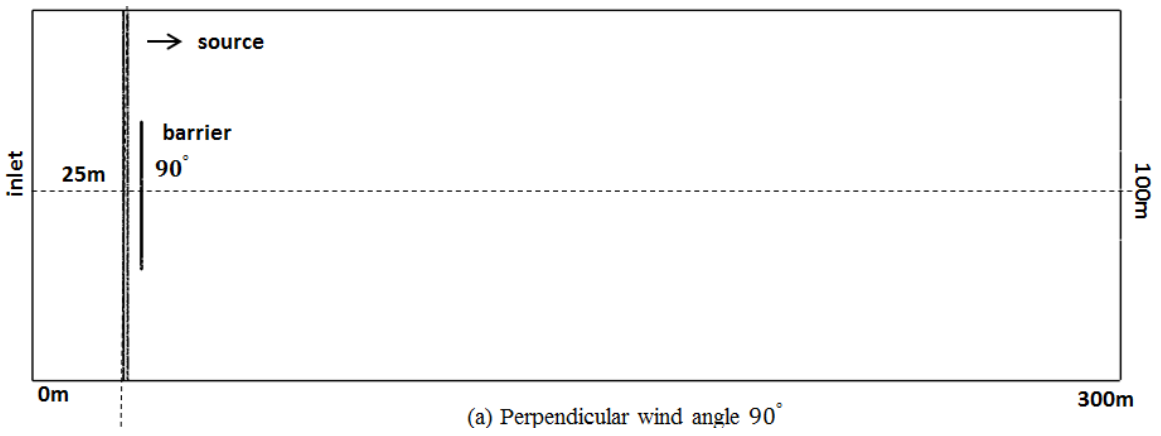

Figure 30: Oblique wind angle computational domain (a) perpendicular wind direction; (b) 75° wind direction; (c) 60°wind direction

Figure 30 Continued

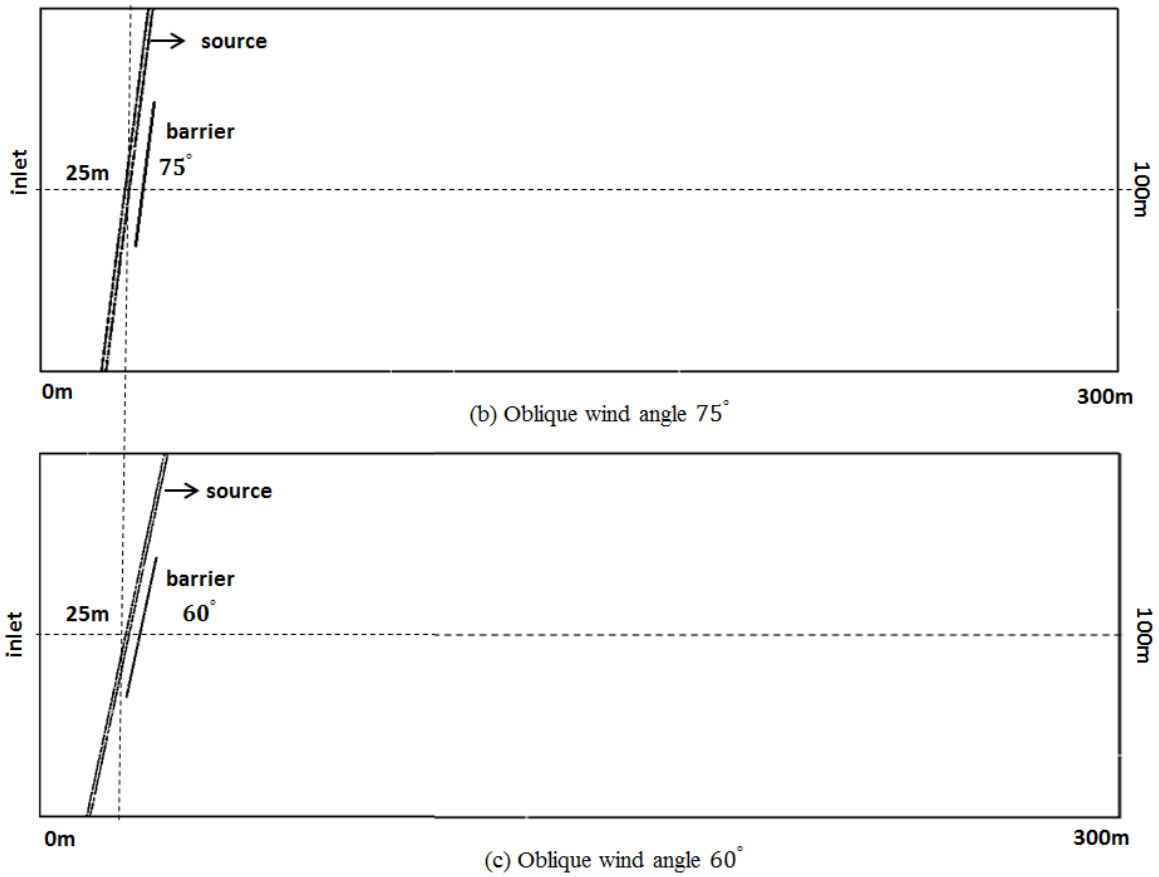

(b) Oblique wind angle 75°

(c) Oblique wind angle 60°

5.2 Flow Characteristic Comparison under Different Oblique Wind and ABL Conditions

This section describes simulation results of 4m single barrier with two oblique angle and perpendicular case. Figure 31 shows velocity streamlines at ground level z=1m for three wind angles under stable, neutral, and unstable conditions.

In general, the results shows consistent trend with non-oblique wind direction. Unstable conditions have the smallest wake region, meaning the faster velocity recovery and bigger turbulence mixing. Due to the existence of barrier edge, downwind flow stream shows asymmetrical pattern following. Under same thermal condition, larger oblique angle case has smaller maximum wind speed overall.

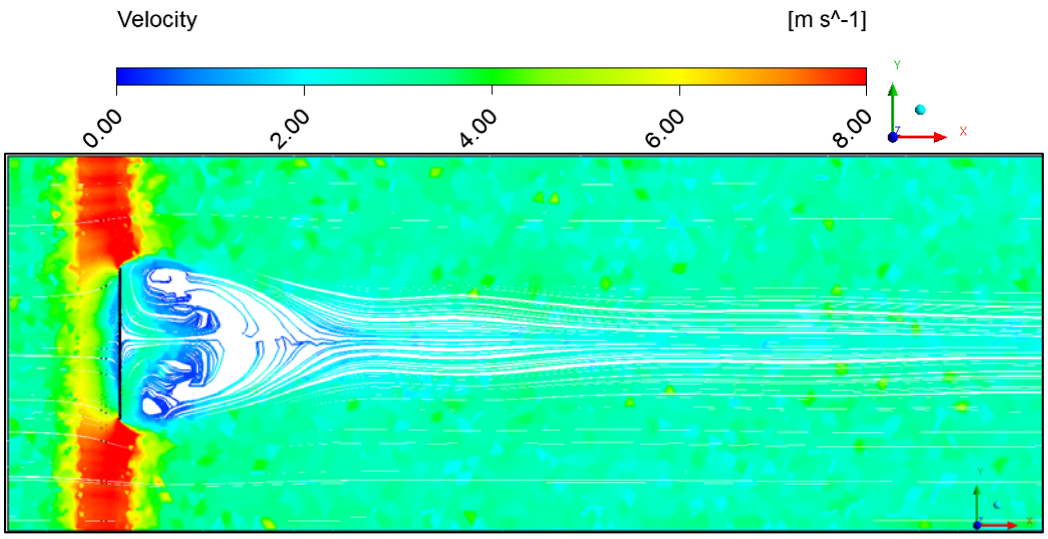

(a) 90° perpendicular to barrier under stable condition

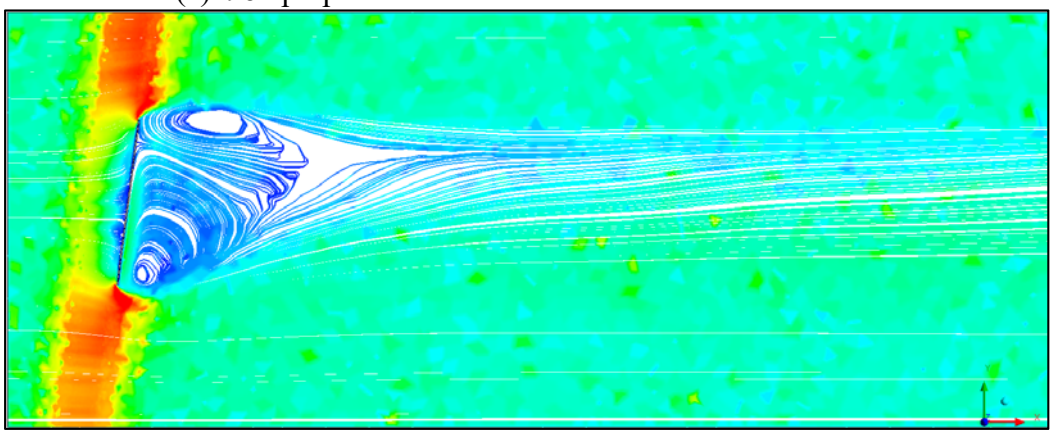

(b) 75° wind oblique to barrier under stable condition

Figure 31: Velocity streamline for oblique wind profiles under different thermal conditions

Figure 31 Continued

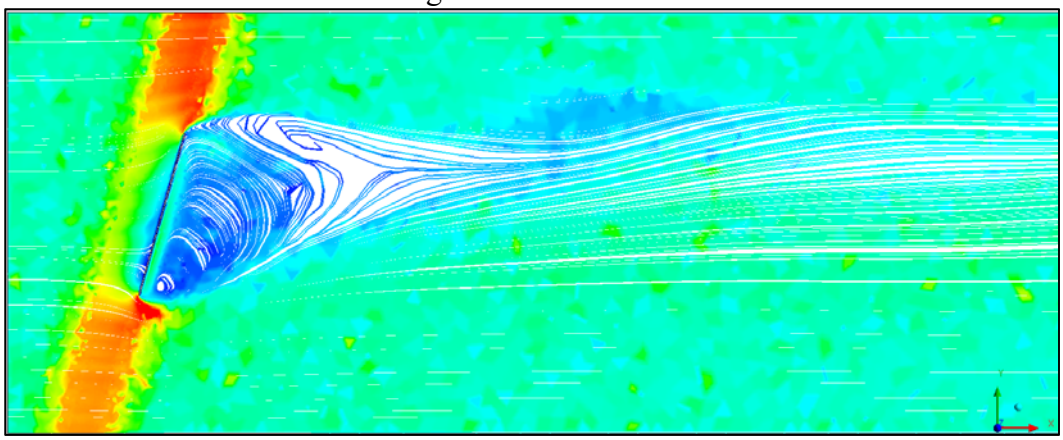

(c) 60° wind oblique to barrier under stable condition

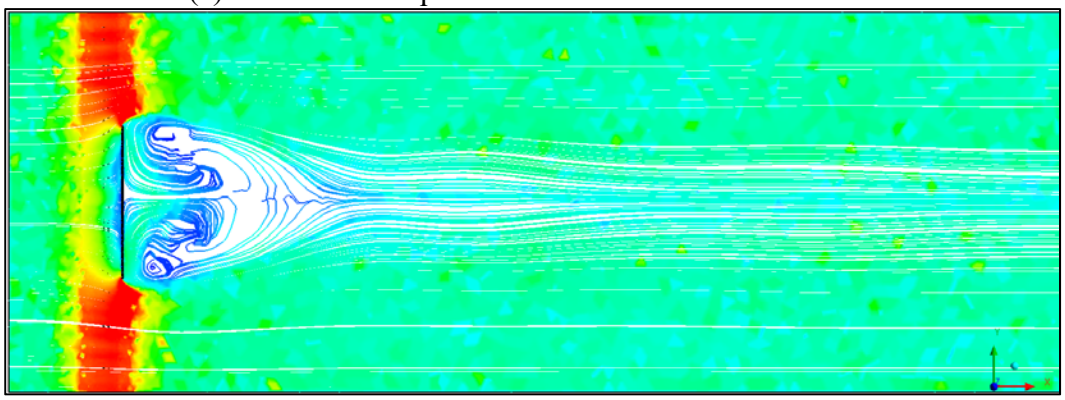

(d) 90° perpendicular to barrier under neutral condition

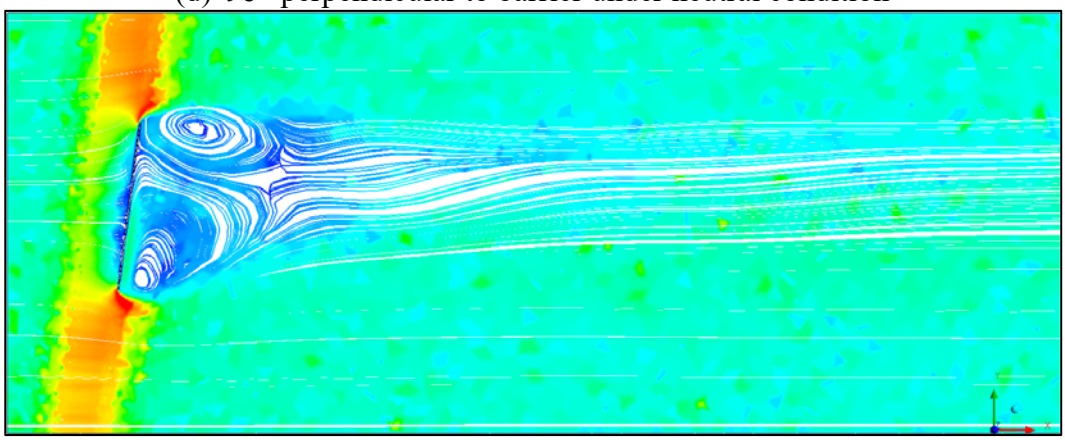

(e) 75° wind oblique to barrier under neutral condition

Figure 31 Continued

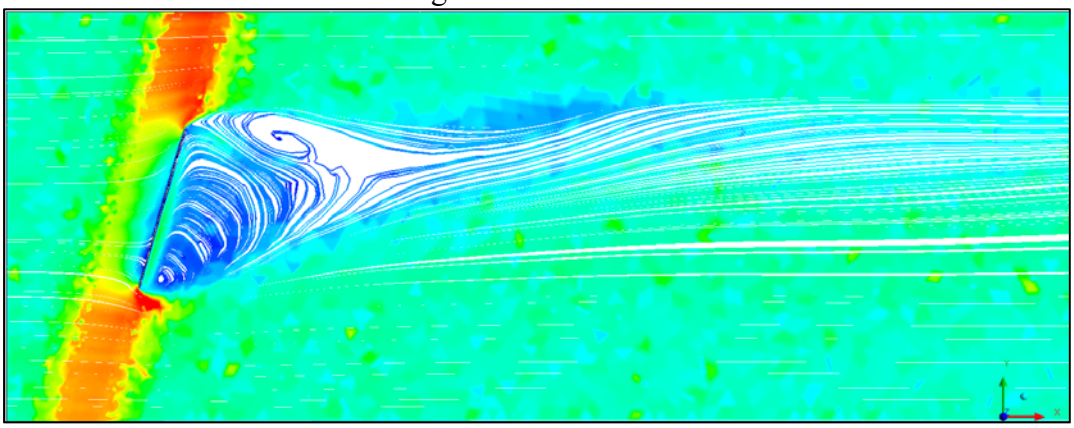

(f) 60° wind oblique to barrier under neutral condition

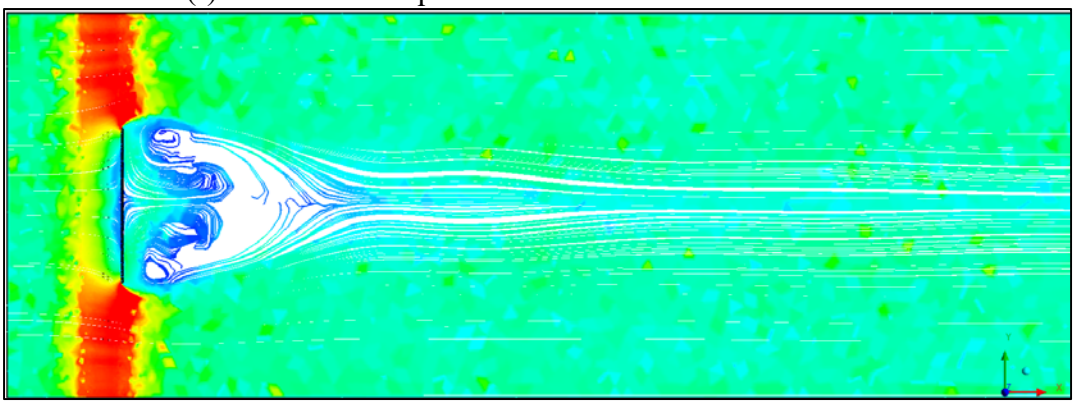

(g) 90° perpendicular to barrier under unstable condition

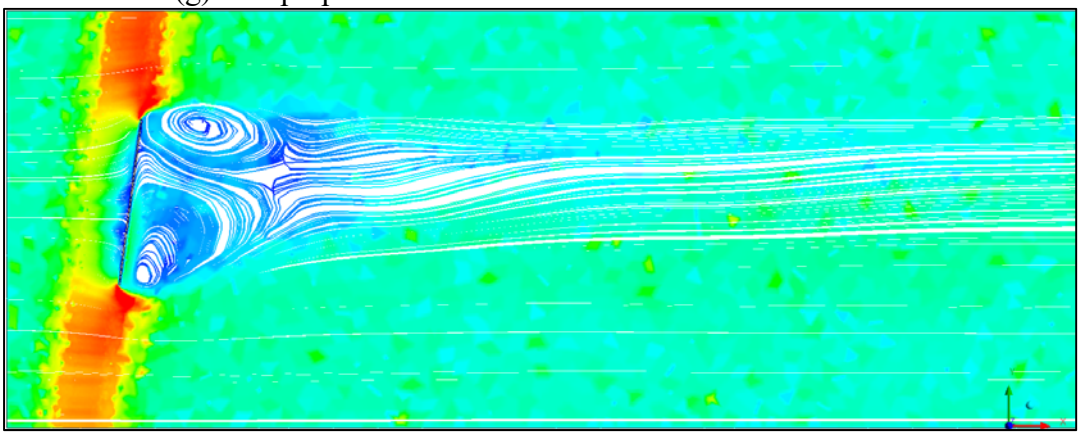

(h) 75° wind oblique to barrier under unstable condition

Figure 31 Continued

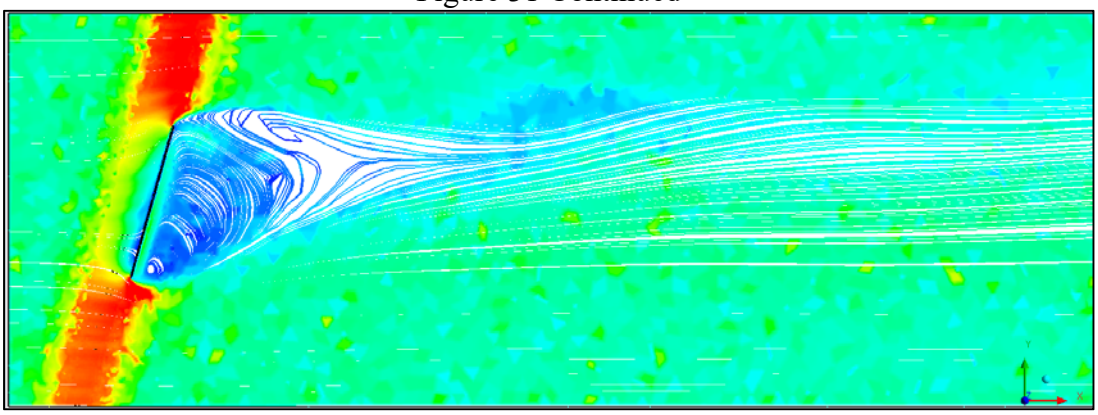

(i) 60° wind oblique to barrier under unstable condition

Figure 32 shows turbulence intensity at ground level z=1m for all cases. as indicated in previous section, turbulence intensity represents turbulence mixing and fluctuation level. Its strength is inverse proportional to pollutant concentration. Under the same thermal condition, larger oblique angle has bigger turbulence intensity near barrier edge and smaller turbulence intensity behind barrier. Barrier edge effects get stronger in oblique wind condition. In unstable condition case, the larger oblique angle of 60° has the biggest turbulence intensity near barrier edge area. The turbulence intensity behind barrier is also bigger than stable and neutral condition cases.

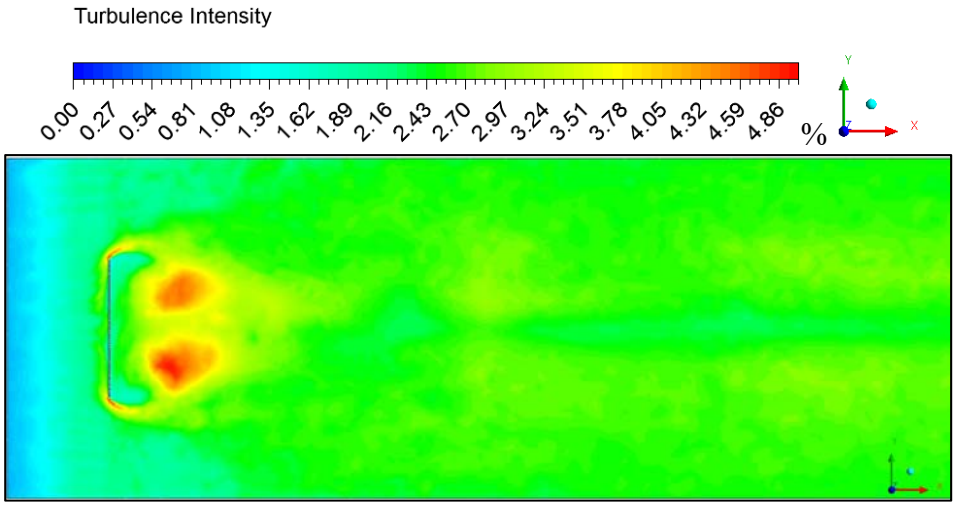

(a) 90° perpendicular to barrier under stable condition

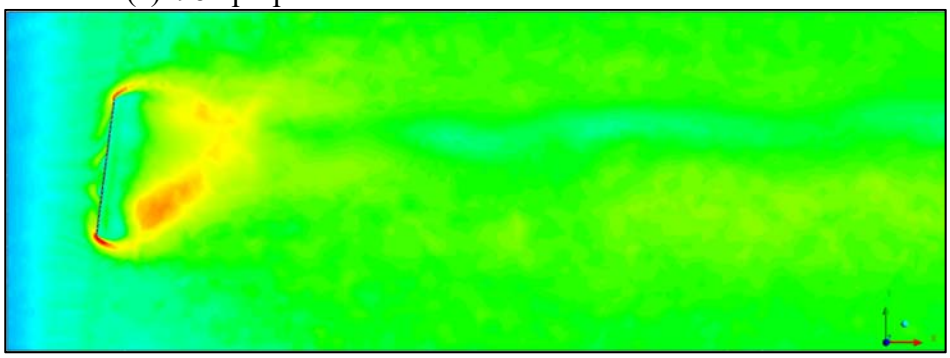

(b) 75° wind oblique to barrier under stable condition

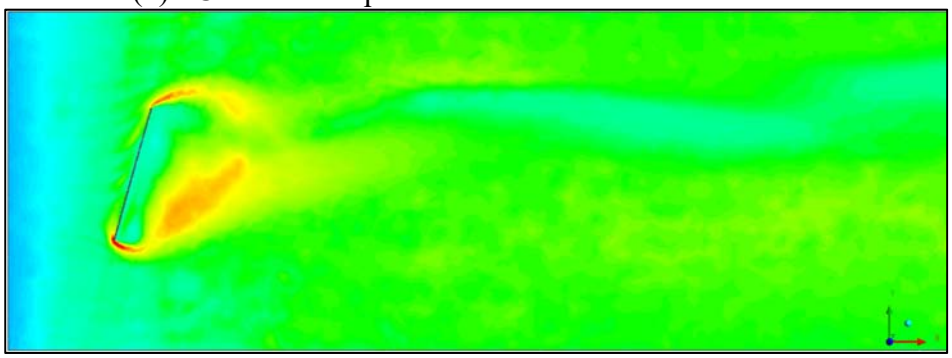

(c) 60° wind oblique to barrier under stable condition

Figure 32: Turbulence intensity at ground level for oblique wind profiles under different thermal conditions

Figure 32 Continued

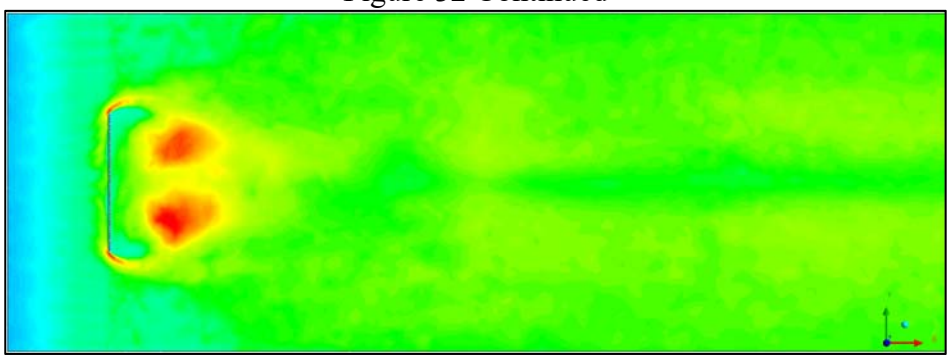

(d) 90° perpendicular to barrier under neutral condition

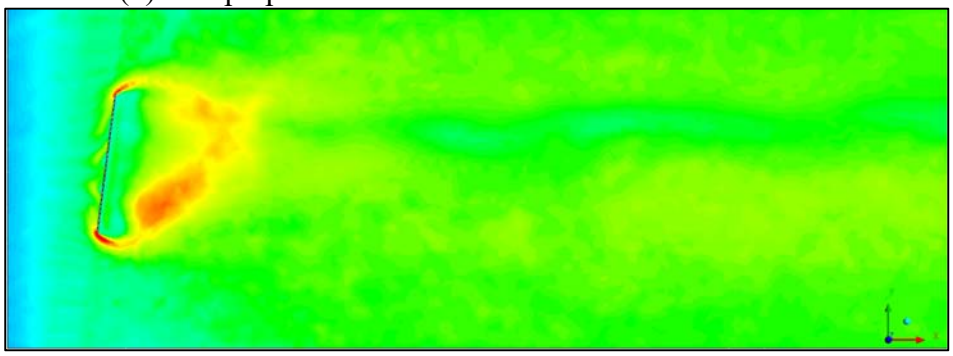

(e) 75° wind oblique to barrier under neutral condition

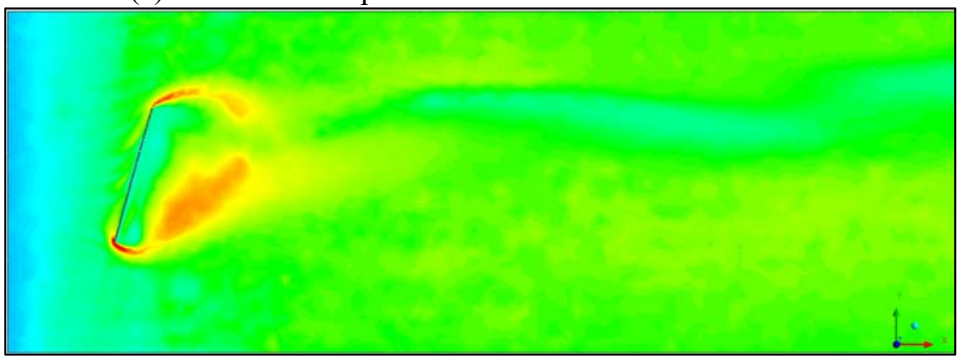

(f) 60° wind oblique to barrier under neutral condition

Figure 32 Continued

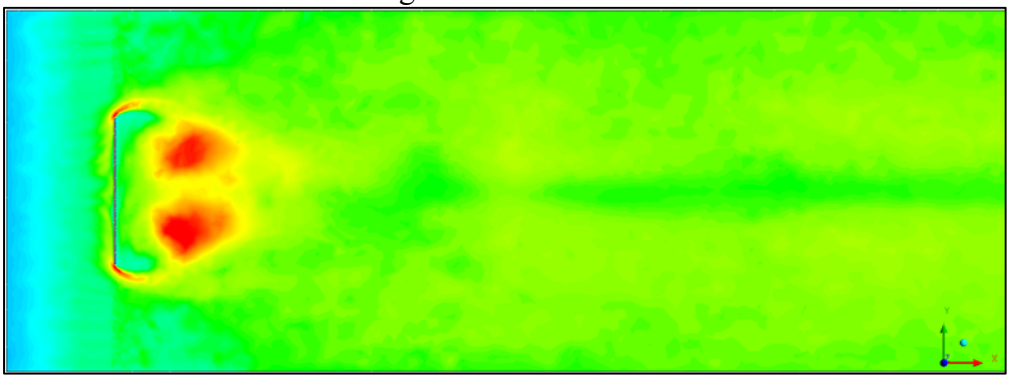

(g) 90° perpendicular to barrier under unstable condition

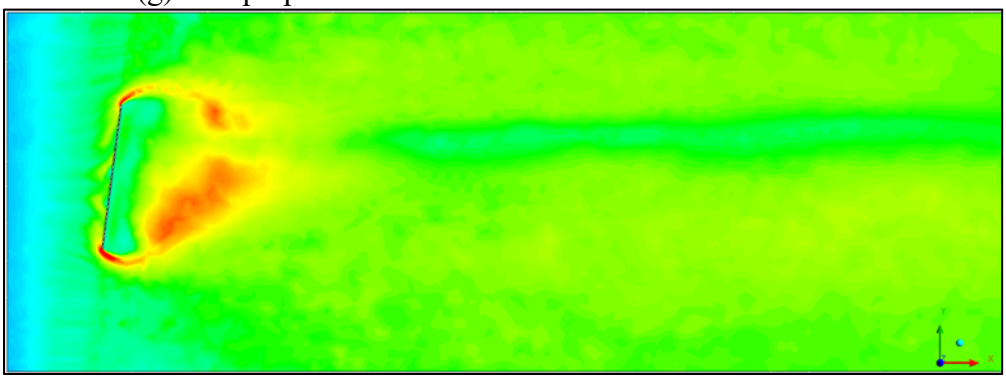

(h) 75° wind oblique to barrier under unstable condition

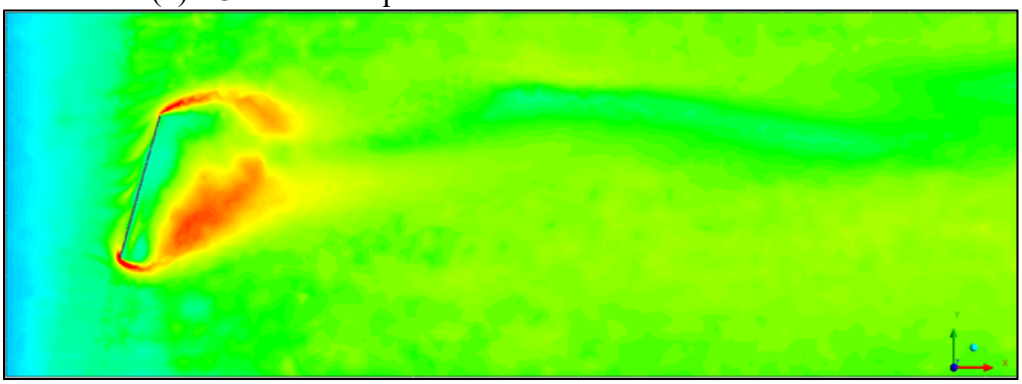

(i) 60° wind oblique to barrier under unstable condition

Figure 33 shows CO_2 concentration at ground level z=1m for three wind angle cases under various thermal conditions. It can be seen that high concentration located at area before barriers on road region. Under the same thermal condition, larger wind oblique angle case has lower downwind concentration. With the same oblique wind angle, unstable condition has the least concentration. Due to oblique angle, concentration distribution also shows asymmetrical pattern.

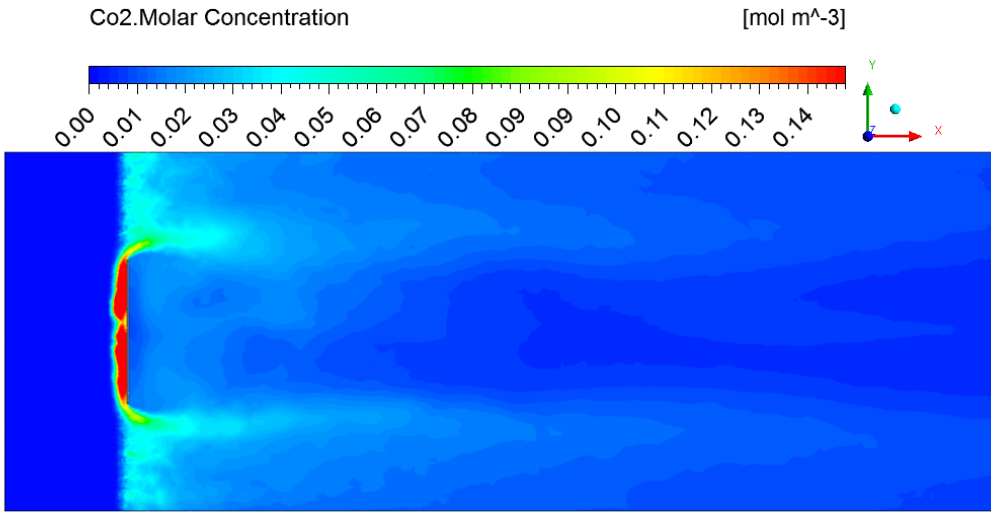

(a) 90° perpendicular to barrier under stable condition

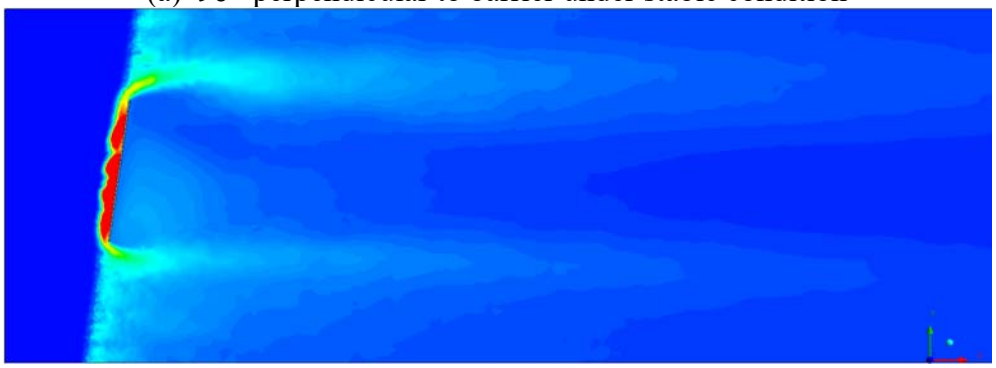

(b) 75° wind oblique to barrier under stable condition

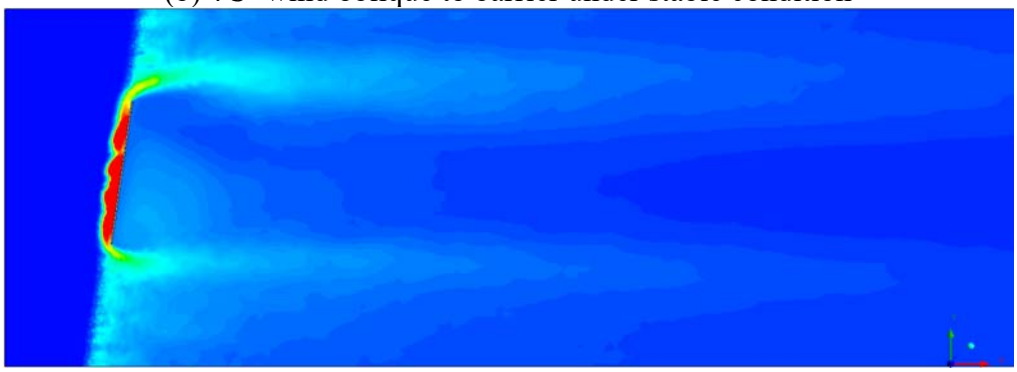

(c) 60° wind oblique to barrier under stable condition

Figure 33: CO_2 concentration contours at ground level for oblique wind profiles under different thermal conditions

Figure 33 Continued

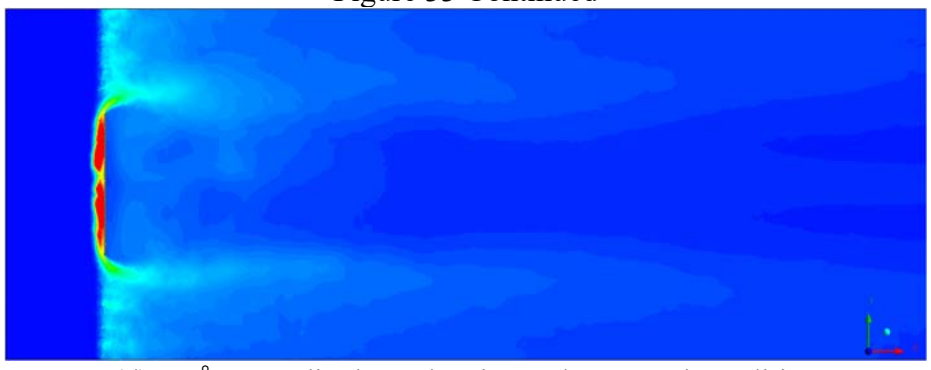

(d) 90 ° perpendicular to barrier under neutral condition

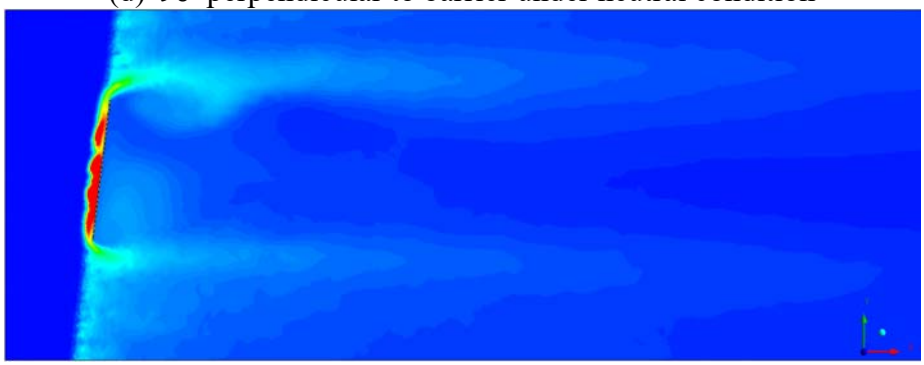

(e) 75° wind oblique to barrier under neutral condition

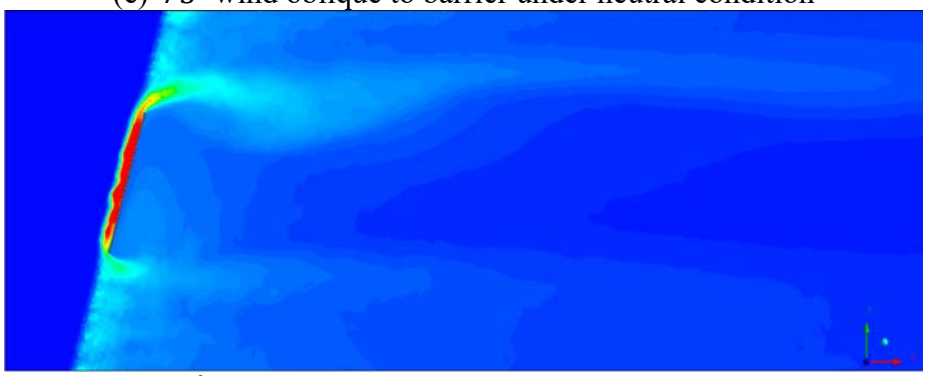

(f) 60° wind oblique to barrier under neutral condition

Figure 33 Continued

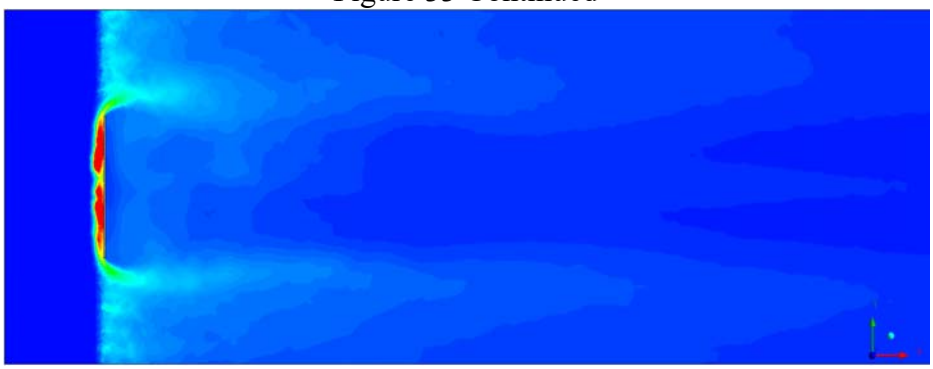

(g) 90° perpendicular to barrier under unstable condition

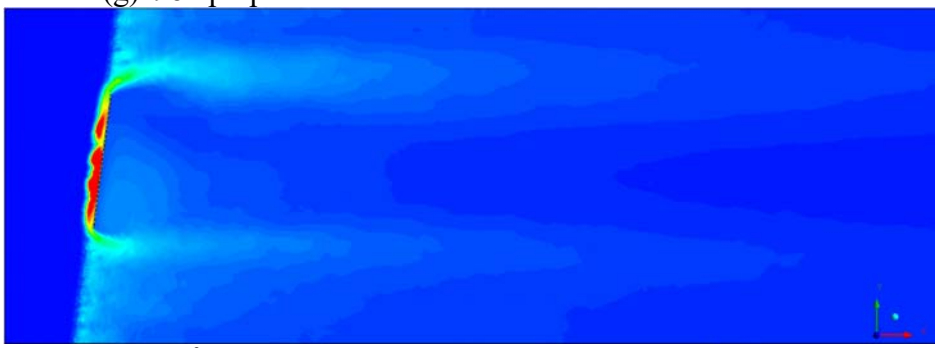

(h) 75° wind oblique to barrier under unstable condition

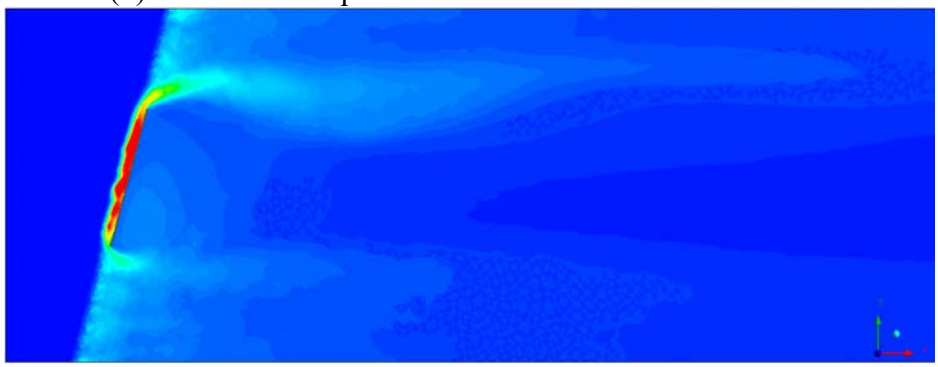

(i) 60° wind oblique to barrier under unstable condition

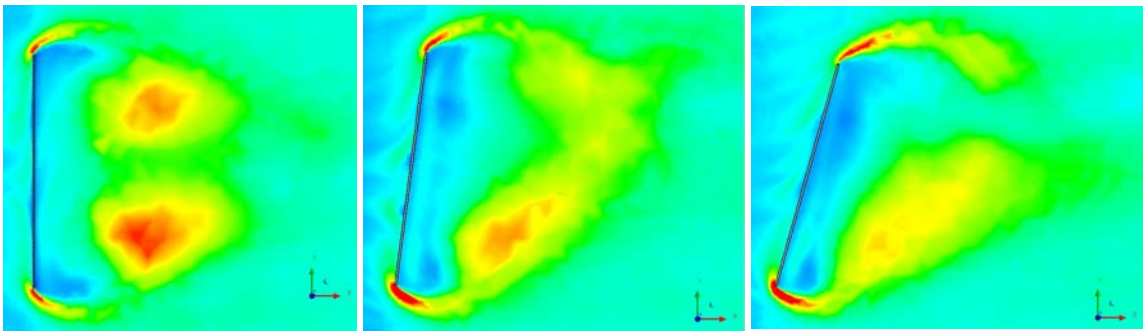

(a) Stable Condition Turbulence Kinetic Energy

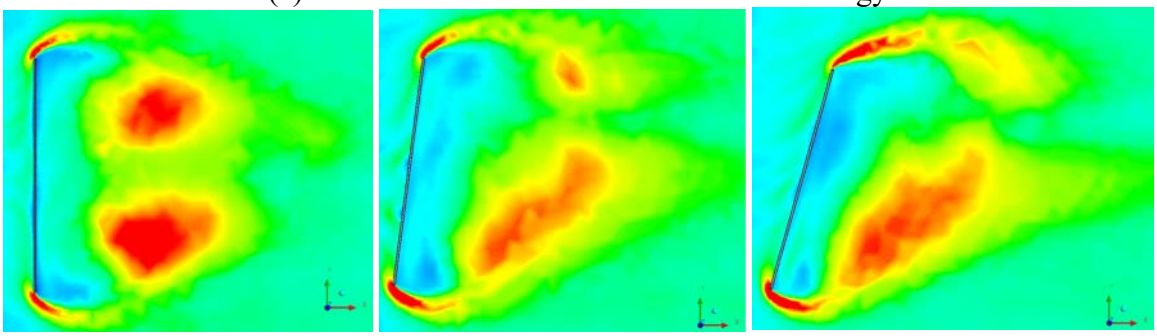

(b) Neutral Condition Turbulence Kinetic Energy

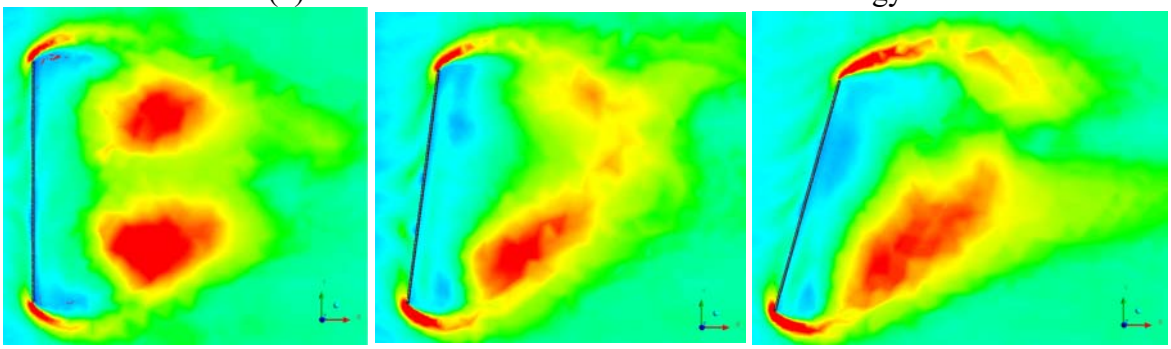

(c) Unstable Condition Turbulence Kinetic Energy

Figure 34: Turbulence kinetic energy (TKE) profile near barrier edge for oblique wind profiles under different thermal conditions at ground level

Figure 34 shows turbulence kinetic energy profile near barrier edge. TKE profile is closely related to turbulence intensity profile. Higher turbulence intensity leads higher turbulence kinetic energy. A bigger TKE can be seen near barrier edge with larger oblique angle.

Figure 35 shows turbulence intensity along line parallel to barrier, which is 1m behind barrier and located at ground level under neutral condition.

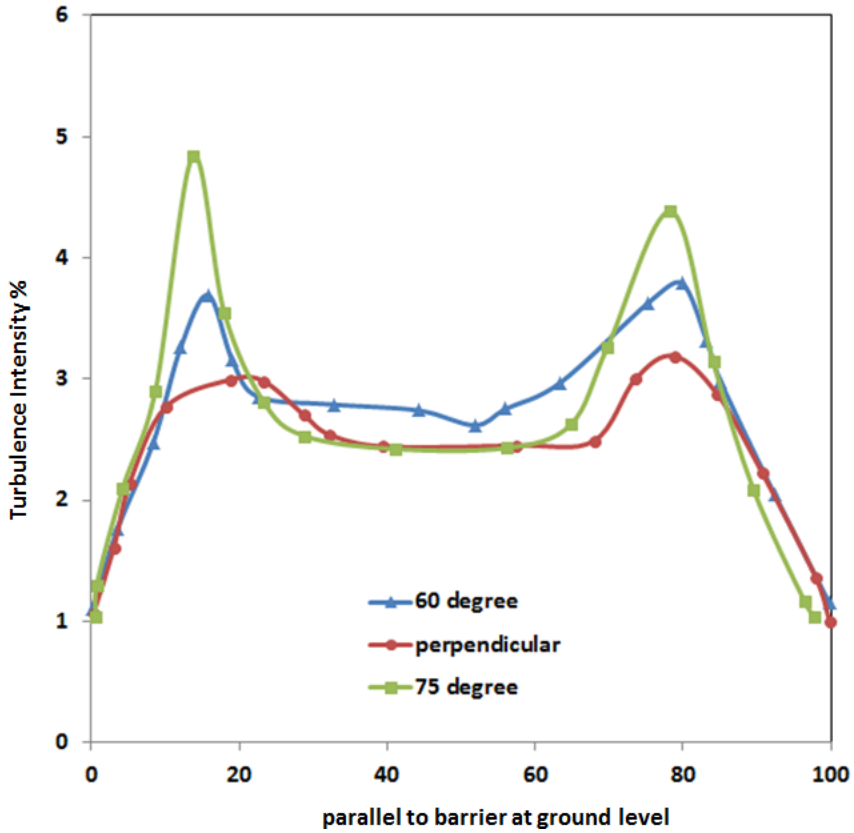

Figure 35: Turbulence intensity along line parallel to barrier located 1m behind barrier at ground level under neutral condition

Results from Figure 35 show turbulence intensity near barrier edges. Higher turbulence intensity can be seen near edges and lower turbulence intensity can be seen in the area between barrier side edges. 75° wind condition has the highest turbulence intensity at two side edges. Perpendicular wind condition has the lowest turbulence intensity.

5.3 Summary of Results

Oblique wind affects flow distribution near barrier edge. The larger the oblique angle is, the stronger effects on turbulence generation near barrier edge. Overall, it is suggested consider oblique wind conditions for further barrier edge effect study.

6. CONCLUSIONS & FUTURE WORK

This project applied numerical method to study roadside noise barrier effects on pollutant dispersion. Study was divided into multiple sections for focusing on different factors. First, simulations were done to validate numerical models with experimental and theoretical results. Similar results were found in our simulations comparing with reference studies. This guaranteed the accuracy of our further simulations.

In the first section, study was focused on noise barrier height effect. Two barrier configurations were studied: downwind single barrier and double barriers. 3D simulation was done using RANS turbulence modeling. Different thermal effects were added. Results confirmed that noise barrier feature can help reduce downwind pollutant concentration up to 300 to 500m far. Overall, double barrier has better performance than single barrier downwind. However, double barrier does have a high concentration accumulation between barriers. In general, the higher is the barrier, the larger reduction in concentration. This is due to the lifting effects on the pollutant dispersion. Noise barrier helps reduce ground level concentration by increasing pollutant vertical span. This impact can be affected by different thermal conditions. Under unstable condition, due to higher turbulence mixing and faster velocity recovery, downwind has the least concentration and smallest wake recovery region. Stable condition has the least turbulence mixing and lower speed, which leads to the highest concentration. These effects can all be explained by turbulence intensity or turbulence kinetic energy, which are representatives of turbulence properties of flow field. In this section, further work can be done by modifying inlet wind profile to log law. And larger domain and finer mesh is expected for more accurate results.

In the second section, barrier edge effect was studied based on double barrier configuration. Barrier side edge effects were first introduced in previous study. However, there wasn’t any research or study focused on this topic. In this study, we applied numerical method simulating different barriers heights with side edge and without side edge to see the edge effects. Thermal effects were also added to this study. Results show that noise barrier edge effect can decrease the performance in reducing downwind pollutant concentration comparing with non-edge effect

barriers. The existence of side edges, a secondary turbulence can mix into the original wake region behind downwind barrier. This secondary turbulence has a vertical direction when it encounters the turbulence induced by barrier top edge. This slows downs the velocity inside wake region can enlarge the wake region. This leads to a larger wake region and a low speed zone behind barrier, which results in a higher pollutant concentration. This impact can also be affected by different thermal conditions. Similar effects can be found for different thermal conditions. Unstable condition has the least downwind concentration and stable condition has the highest concentration. Study was done to different barrier heights. It was shown that the higher is the barrier, the stronger the edge effects can be. Edge effects can be visualized by seeing the downwind pollutant concentration distribution. At 1m barrier, downwind concentration distribution has similar shape as non-barrier case. As barrier height increases, downwind concentration distribution starts to show a similar Gaussian distribution shape. Closer to downwind barrier, concentration distribution does not follow Gaussian shape. This can be explained by edge effect induced turbulence flow mixing. In this section, further work can be done by simulating more barrier heights. Larger domain of longer barrier can give us a deeper look at edge effect when the effect can be ignored, and when the effect is very important to take into consideration.

In the last section, simulations were done to study edge effects with oblique inlet wind profile. It was shown that edge effect gets stronger under oblique wind condition. Results also show that larger oblique wind angle has a smaller downwind concentration. This effect can be seen further downwind comparing with perpendicular case. Further study of this topic will focus on applying moving mesh and simulate different oblique angles.

Overall, this study used numerical simulation method studied multiple topics about noise barriers feature ability to help reduce downwind pollutant concentration. More representative vehicle emission gases should be taken into consideration for future work. Vehicle induced turbulence is another critical factor that affects the accuracy of this study. Advanced method in modeling vehicle induced turbulence and add that factor into simulation will be another area to explore.

REFERENCES

[1] Pressbooks Accessible online: https://ohiostate.pressbooks.pub/sciencebites/chapter/causes-and-consequences-of-air-pollution-in-beijing-china/.

[2] EPA. Accessible online: https://www.epa.gov/newsreleases/us-epa-partners-study-roadside-vegetation-and-air-quality-local-school.

[3] EPA. Accessible online : https://www.epa.gov/sites/production/files/2015-10/documents/ochp_2015_near_road_pollution_booklet_v16_508.pdf.

[4] D.K.Heist.; S. G. Perry.; L.A. Brixey. A wind tunnel study of roadway configurations on the dispersion of traffic-related pollution. *Atmopsheric Environment*. 2009. Volume 43. Pages 5101-5111. https://doi.org/10.1016/j.atmosenv.2009.06.034.

[5] R. Baldauf.; E. Thoma.; A. Khlystov.; V. Isakov.; G. Bowker.; T. Long.; R. Snow. Impacts of noise barriers on near-road air quality. *Atmospheric Environment.* 2008. Vol. 42 Pg. 7502–7507.

[6] Z. Ning.; N. Huddaa.; N. Dahera.; W. Kam.; J. Herner.; K. Kozawa.; S. Mara.; C. Sioutas. Impact of roadside noise barriers on particle size distributions and pollutants concentrations near freeways. . *Atmopsheric Environment*. 2010 Volume 44, Issue 26, Pg. 3118-3127. DOI: https://doi.org/10.1016/j.atmosenv.2010.05.033.

[7] Gayle S.W.Hagler.; M.Y. Lin. ; A. Khlystov.; R. W. Baldauf. ; V. Iskov.; J. Faircloth.; L. E. Jackson. Field investigation of roadside vegetative and structural barrier impact on near-road ultrafine particle concentrations under a variety of wind conditions. Science of Total Environment. 2012. VOL. 419. Pg. 7-15

[8] D. Finn.; K.L. Clawson.; R.G. Roger.; J.D. Rich.; R.M. Eckman.; Tracer studies to characterize the effects of roadside noise barriers on near-road pollutant dispersion under varying atmospheric stability conditions. *Atmosphere Enviroment*. 44(2):204-214

[9] R. W. Baldauf.; V. Iskov.; P. Deshmarkh.; A. Venkatram.; B. Yang.; K. M. Zhang. Influence of solid noise barriers on near-road and on-road air quality. *Atmospheric Environment.* 2016. VOL 129. Pg. 265-276.

[10] Gayle S.W. Hagler.; W. Tang.; M. J. Freeman.; D. K. Heist.; Steven. J. Perry.; A. F. Vette. *Atmospheric Environment.*2011. VOL. 45. Pg. 2522-2530.

[11] N. Schulte.; M. Snyder.; V. Isacov.; D. Heist.; A. Venkatram. *Atmospheric Environment.* 2014. VOL. 97. Pg. 286-295. DOI: https://doi.org/10.1016/j.atmosenv.2014.08.026.

[12] Lee, Eon S.; Ranasinghe, Dilhara R.; Ahangar, Faraz Enayati; Amini, Seyedmorteza; Mara, Steven; Choi, Wonsik; Paulson, Suzanne; Zhu, Yifang. *Atmospheric Environment.*2018. VOL. 175. Pg. 92-99.

[13] Amini, S., F. Ahangar, D. Heist, S. Perry, AND A. Venkatram. *Atmospheric Environment.* Modeling Dispersion of Emissions from Depressed Roadways. *Atmospheric Environment. 2018.* VOL. 186. Pg. 189-197. DOI: https://doi.org/10.1016/j.atmosenv.2018.04.058

[14] Jonathan T. Steffens.; David K. Heist.; Steven G. Perry.; K. Max Zhang.; Modeling the effects of a solid barrier on pollutant dispersion under various atmospheric stability conditions. *Atmospheric Environment.* 2013 VOL. 69. Pg.96-85.

[15] M. Ghasemian; S. Amini; M. Princevac. The influence of roadside solid and vegetation barriers on near-road air quality. *Atmospheric Environment. DOI: 10.1016/j.atmosenv.2017.09.028.*

[16] J.E. Pieterse.; T.M. Harms. *Journal of Wind Energy and Industrial Aerodynamics.* October 2013, . Volume 121, Pages 82-97

[17] C. Alinot.; C. Masson. Aerodynamic Simulations of Wind Turbine Operating in Atmospheric Boundary layer with Various Thermal Stratifications. 2002 ASME Wind Energy Symposium Reno,NV,U.S.A.

[18] ANSYS, 2017. ANSYS FLUENT 18.1 Theory Guide. 14.1.1 Species Transport Equation. Executive summary. Light-Duty Automotive Technology, Carbon Dioxide Emissions, and Fuel Economy Trends:1975 Through 2017. EPA, EPA-420-S-18-001 January 2018.

[19] EPA PDF. Accessible online: https://www.epa.gov/fuel-economy-trends

[20] Amini S. Faraz.E. A. Nico S. Akula. V. Using models to interpret the impact of roadside barriers on near-road air quality. *Atmospheric Environment.* 2016. DOI: 10.1016/j.atmosenv.2016.05.001

[21] M. Abkar.; F. Porte-Agel. Influence of Atmospheric Stability on Wind-Turbine Wakes: A Large-Eddy Simulation Study. *AIP Physics of Fluids*. 27, 035104 (2015). DOI: 10.1063/1.4913695